Bioinspired surfaces with superamphiphobic properties : concepts, synthesis, and applications

Liu, Hui; Wang, Yandong; Huang, Jianying; Chen, Zhong; Chen, Guoqiang; Lai, Yuekun

2018

Liu, H., Wang, Y., Huang, J., Chen, Z., Chen, G., & Lai, Y. (2018). Bioinspired surfaces with superamphiphobic properties : concepts, synthesis, and applications. Advanced Functional Materials, 28(19), 1707415-. doi:10.1002/adfm.201707415

https://hdl.handle.net/10356/106258

https://doi.org/10.1002/adfm.201707415

Article type: Review

Bioinspired surfaces with superamphiphobic properties: Concepts, synthesis and applications

Hui Liu, Yandong Wang, Jianying Huang*, Zhong Chen, Guoqiang Chen, and Yuekun Lai**

H. Liu, Prof. J. Y. Huang, Prof. G. Q. Chen, Prof. Y. K. Lai
National Engineering Laboratory for Modern Silk, College of Textile and Clothing Engineering, Soochow University, Suzhou 215123, China.
E-mail: yklai@suda.edu.cn; jyhuang81@suda.edu.cn
Prof. Y. D. Wang
Institute of Functional Nano & Soft Materials (FUNSOM) and Jiangsu Key Laboratory for Carbon-Based Functional Materials & Devices, Soochow University, Suzhou 215123, China.
E-mail: wangyandong@suda.edu.cn
Prof. Z. Chen
School of Materials Science and Engineering, Nanyang Technological University, 50 Nanyang Avenue, 639798 Singapore, Singapore.

Abstract: Among diverse wetting phenomena in surface science, superamphiphobicity is regarded as one of the most special super-antiwetting states. In this paper, a systematic summary has been generated to cover the characterization of surface wettability, the construction techniques, and selected functional applications. With respect to fabrication techniques, we will discuss the following three types of technology routes, viz., 'pre-texturing + post-modifying', 'pre-modifying + post-texturing', and in-situ one-step construction. Discussion has been made on the merits and demerits of each technology route. It is vital to rationally design or adopt appropriate construction strategies in diverse conditions. Appropriately constructed superamphiphobic multifunctional surfaces can be applied in many fields, however, most have not been scale-up and utilized for practical

applications due to some specific difficulties required to be resolved in the future. These challenges and further outlook for super-antiwetting surfaces are discussed in this review.

Keywords: superamphiphobicity, wettability, re-entrant geometries, construction strategies, applications

1. Introduction

As a common phenomenon in our daily life, wetting can be widely observed everywhere from macroscopic scene to microcosmic world, such as high tides on the beach and ion channels in cell membranes.[1-3] Wettability is considered as one of the most fundamental properties to define the contact between a liquid and a solid surface, which has been playing a significant role in almost all sectors of our economy. Since Young's equation was introduced in 1805,[4] areas on wetting and wettability have been studied for more than two centuries. Nowadays, super-antiwetting property, including superhydrophobicity, superoleophobicity, and superamphiphobicity, has received a great deal of attention. [5-12] Superamphiphobicity refers to the state that possesses contact angles higher than 150° and sliding angle lower than 10° for both water and oil. Dating back to more than a century ago, the initial study on super-antiwetting surface with an extraordinarily high CA close to 180º was firstly carried out by Ollivier who used soot to fabricate coatings on a substrate in 1907.[13] Afterwards in 1953, Bartell et al. constructed paraffin-covered surfaces with microscale pyramids, which displayed outstanding repellency to water.[14] Thereafter,

the so-called superhydrophobicity gained continual but relatively circumscribed attention until 1997 when Barthlott and Neinhuis put forward the origin and the general theory of the famous 'lotus effect'.[15] The epicuticular wax and micro/nano-scale dual structures on the surface were revealed to be responsible for the superhydrophobic property. Since then, many researchers have devoted to fabricating artificial superhydrophobic materials with similar micro/nano-structures by imitating various plant and animal structures.[5, 16]

The aforementioned principle also applies to oil-repellent property, known as the superoleophobicity.[17, 18] In contrast to common superhydrophobic surfaces, the superoleophobic surfaces can repel not only oil but also water for the fact that oil liquids possess much smaller surface free energy, for example, the surface energy of decane is 23.8 mN m^{-1}, which is much lower than that of water (72.3 mN m^{-1}). Therefore, superoleophobic surfaces should display superamphiphobic properties or simply denote as "superamphiphobic".[18] However, technically it is still a challenge to achieve such super-antiwetting materials, especially when the surface energy of the oil is very low. In 2007, Tuteja et al. firstly developed superoleophobic surfaces by introducing the re-entrant surface feature, which is different from the conventional approach of adjusting the surface roughness.[17] So far, it has been well established that the suitable surface roughness or surface feature in conjunction with low surface energy materials are the two essential elements to fabricate superamphiphobic surfaces (**Figure 1**), and this has been the foundation for almost all the development of superamphiphobic surfaces in recent years.[19-22] With the competence of building

the superamphiphobic surfaces, a wide range of application-driven researches have emerged in recent years, such as oil-water separation, self-cleaning, anti-icing, anti-fouling, patterning, droplet-manipulation and so on.[23-29]

In this review, we will focus on the progress of superamphiphobic surfaces. Then in the following sections, we will first introduce some typical creatures with special wettabilities in nature from which inspiration has been drawn for the development of superamphiphobic materials, followed by the analytical methods for wettability studies. Subsequently, we will review some common fabrication methods and potential applications. In the end, we will conclude the review with a brief outlook in this field of research, based on the summarized current challenges and potential solutions in the future.

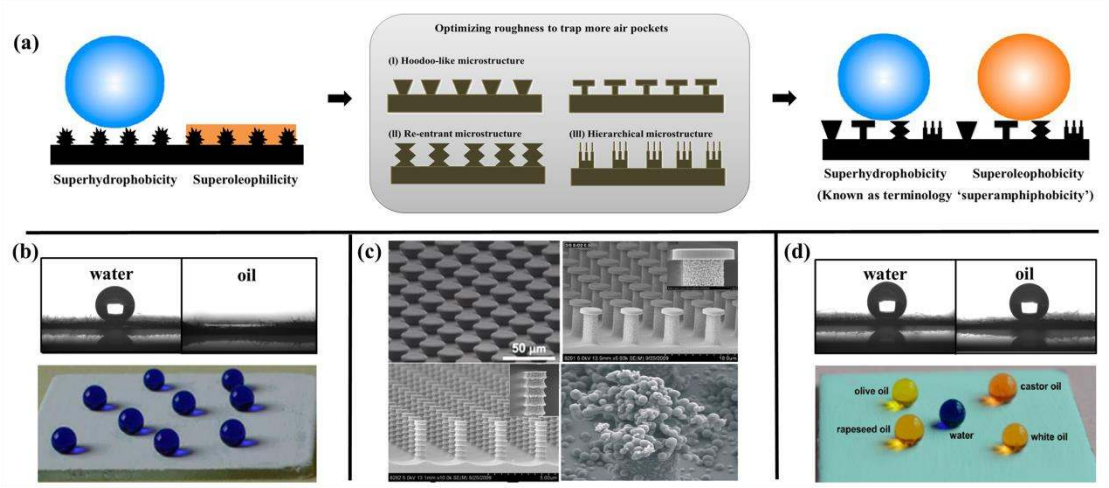

Figure 1. (a) Increasing the surface roughness and reducing the surface energy are two key factors to fabricate superamphiphobic surface (i.e., simultaneously superhydrophobic and superoleophobic surface). Modifying the surface with low surface-energy molecules. Introducing hoodoo-like, re-entrant or hierarchical microstructures to trap more air pockets and to pin the liquid/solid contact lines to

prevent the permeation of water and oil droplets. Reproduced with permission from [27]. Copyright 2015 American Chemical Society. (b) The CAs of water an oil on superhydrophobic and superoleophilic surfaces and corresponding images. Reproduced with permission from [29]. Copyright 2016 American Chemical Society. (c) Corresponding SEM images of hoodoo-like, re-entrant or hierarchical microstructures. Reproduced with permission from [30]. Copyright 2010 The Royal Society of Chemistry. Reproduced with permission from [31]. Copyright 2012 American Chemical Society. Reproduced with permission from [32]. Copyright 2015 American Chemical Society. (d) The CAs of water an oil on superhydrophobic and superoleophilic surfaces and corresponding images. Reproduced with permission from [29]. Copyright 2016 American Chemical Society.

2. Natural creatures with special wettability

In order to acclimatize themselves to natural environment, many plants and animals in nature have developed particular morphology and structures during long-time evolution. In recent years, breakthroughs in understanding the fundamental reasons behind the natural superhydrophobic and superoleophobic surfaces have led to numerous biomimetic researches following the features of gecko setaes, butterfly wings and so on.[33,34] In particular, various classic examples with oil-repellent surfaces in nature (in air) have been studied.[35] For instance, Aizenberg et al. observed that bacterial (Bacillus subtilis) biofilm colonies and pellicles (**Figure 2**a) exhibit persistent anti-wetting property to many liquids with low surface tension.[36]

Gorb's group has reported oil repellency of leafhoppers, whose integuments were uniformly and densely covered with many bronchosomes, a kind of highly structured particles (**Figure 2**b).[37] As one of the most significant and attractive natural organisms with oil-repellency, the springtails (also called collembolan) were found by Werner et al. to easily survive in water and even oil environments without suffocating.[38-41] The robust surface plastrons composed of hexagonal or rhombic comb-like patterns or secondary granules with hexagonal basic patterns can be observed on their cuticle structures. After immersing the springtails in water and oil, the surfaces were covered with an obvious layer of protective air cushion, typical for a superamphiphobic surface. This group of researchers has systematically investigated the cuticle micro- or nano-morphology of about 40 various springtails (**Figure 2**c–f) and came to a conclusion that the combination of multiscale roughness (e.g., the re-entrant topography) and chemical composition (e.g., chitin or protein) has endowed these springtails with extreme oil-repellency in air. The inspiration from these oleophobic surfaces in nature has paved the way for more examples of oil-repellent surfaces.[42-44]

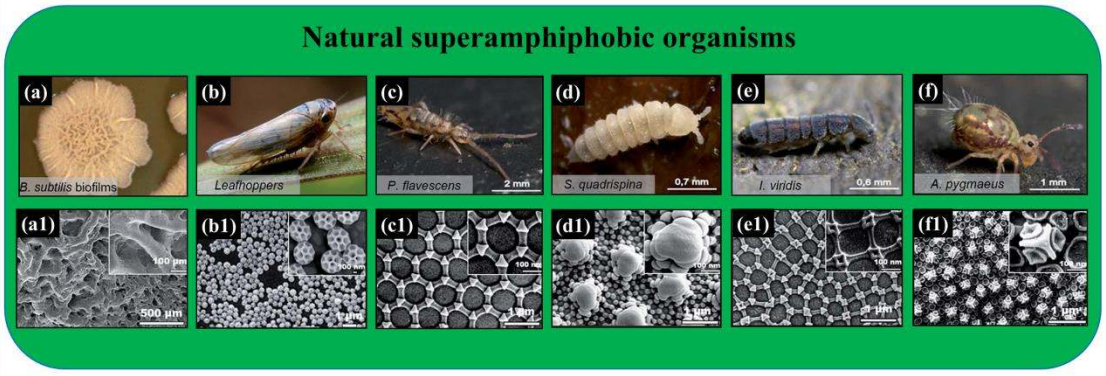

Figure 2. Habitus images and respective morphological characteristics of

representative oil-repellent examples in nature. (a, a1) Bacterial biofilms of Bacillus subtilis [36] (copyright 2011 National Academy of Sciences). (b, b1) Leafhoppers [37] (copyright 2012 the author(s); published by the Royal Society). (c–f) Different spices of springtails [40] (copyright 2012 Springer-Verlag Berlin Heidelberg).

3. Fundamental understandings of superamphiphobicity

3.1. Characterization of wettability

A sessile drop will normally form in the shape of a sphere sectioned by the surface when it is placed on a flat substrate. There is a discrete and measurable contact angle θ_{CA} between the sphere and the surface at the circular solid–liquid–vapour three-phase contact line. In general, a hydrophilic surface displays $\theta_{CA} < 90^{o}$, while hydrophobicity means $\theta_{CA} > 90^{o}$. Particularly, if a surface possesses θ_{CA} larger than 150^{o}, as well as a sliding angle θ_{SA} lower than 10°, it is specified as a super-repellant surface. The surface that only repels water is regarded as superhydrophobicity, whereas the surface deemed as superamphiphobicity can display super-antiwetting property towards both water and various oil liquids with lower surface energy than water. To investigate the superamphiphobic properties, the characterization is important. Eye visualization, as the simplest approach, is always applied to identify a super-antiwetting surface. By this method, the wetting and flowing behaviours can be visualized when a gentle flow of a probing liquid is employed to the surface. The surface is acknowledged as superamphiphobic if not only water but also the oils can move easily along it. However, to make a precise

distinguish among different super-repellent properties, static contact angle and contact angle hysteresis have to be measured by accurate professional equipment.

3.1.1. Static contact angle

Classically, the surface wettability is assessed by the static contact angle as described by Young's equation (**Figure 3**a). When a fluid droplet gets in touch with a surface, the contact angle can be regulated by a combination of interfacial tensions between the solid–liquid (γ_{SL}), solid–vapour (γ_{SV}) and liquid–vapour (γ_{LV}) interfaces:

$$\cos\theta_{CA} = \frac{\gamma_{SL} - \gamma_{SV}}{\gamma_{LV}} \quad (1)$$

However, the aforementioned Young's equation[4] is applicable only for flat and smooth surfaces, losing sight of the real interactions between droplets and substrates and some other external forces in practical situations.[45] However, such ideal surface does not exist in reality. Hence, contact angles on a rough surface usually display variation because of the more complicated solid–liquid interactions. In order to better expound this phenomenon, two different models have been developed to describe the water contact in the Wenzel regime [46] and Cassie–Baxter regime.[47] In the Wenzel regime, both wettability and non-wettability can be promoted because of surface roughness, depending on the chemical properties of the surface (**Figure 3**a,b). In this regime, the relationship between the measured θ_{CA} and the 'true' contact angle of a flat surface (θ_{flat}) is described as follows:[53]

$$\cos\theta_{CA} = R \cdot \cos\theta_{flat} \quad (2)$$

where R is the ratio of the actual surface area of the rough surface to the apparent area.

Stable air pockets may present in rough interstices between the droplets and surfaces, leading to a composite liquid-vapour-solid interface and thereby a more anti-wetting surface, which case is deemed as Cassie–Baxter regime.[53]

$$\cos\theta_{CA} = -1 + \emptyset_S \cdot (1 + cos\,\theta_{flat}) \quad (3)$$

where $\emptyset_S$ is the fraction of the surface that is in contact with the liquid. In such state, the liquid rests only partial surface with very finite contact region. Compared with the flat surface, the contact angles of rough surface made up of the same materials are always much larger because of the trapped air in the pores. Therefore, surface morphology plays a very key role in the wettability.

The above-mentioned states are always regarded as two extreme situations, in which droplets sit on the super-repellent surfaces. Nevertheless, some intermediate states like ‘‘petal’’ state,[48] ‘‘gecko’’ state[49] and metastable Cassie state,[50] also exist in special cases, in which droplets may partially wet the roughed surfaces (**Figure 3**c). On the surface of a rose petal, the droplet permeates into the textured structure, partially wetting the surface. It can be observed that the micropapillaes in large scale on the petal surface are impregnated by droplets, while the nanofolds on top of the micropapillaes still keep unwetted. In this wetting case, the droplets can stick firmly to the surfaces of petal even when they are placed upside down. In addition, another wetting state with high adhesion named the ‘‘gecko’’ state describes a negative

pressure between water droplet and the surface caused by the sealed air pockets trapped in the nano-space, resulting in a high adhesive force. The metastable Cassie state, as the name suggests, is not a real equilibrium state. Such a state originates from a superoleophobic surface with local curvature. Though these surfaces display liquid CA more than 90^{o} and have low surface tension, the interface between air and liquid on the textured surface is pinned by the local surface curvature, preventing the liquid from infiltrating into it and resulting in the superoleophobic property.[51-54] However, an outer interference may induce the surface to transit from the metastable Cassie state to the Wenzel state and lead to the loss of its superoleophobicity.

It is worthy of notice that the liquid-infused surface has been recently developed to liquid-repelling one. Nevertheless, the Wenzel and Cassie–Baxter equations are not suitable to explain its repellency. Rather, the liquid-infused surface has eliminated adhesion between the droplet and the substrate in virtue of its liquid surface rather than the micro/nanoscale structures to repel fluids. The oil liquids with extremely low surface energy can produce a stable and smooth interface, restricting most liquids from permeating and at the same time resisting the adhesion of a variety of matters.[55]

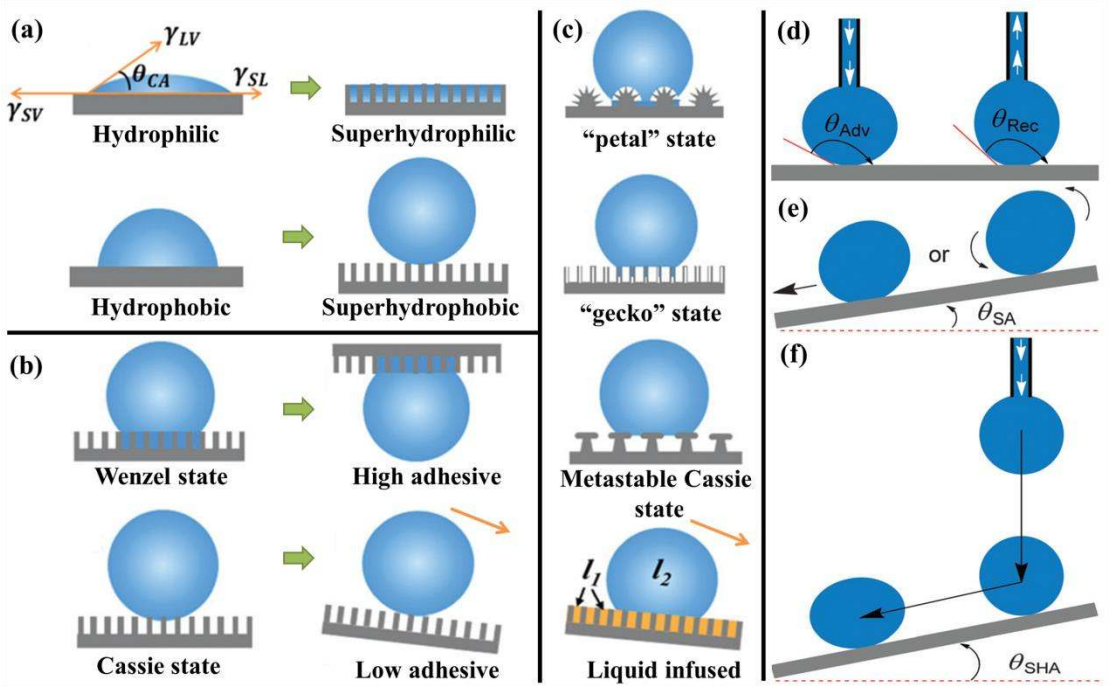

Figure 3. (a) Rough structures can enhance surface wettability. (b) The droplet with high adhesive force in Wenzel state can firmly adhere to the substrate surface even when it is reversed downwards. The droplet with low adhesive force in Cassie state can easily roll down the substrate. (C) Several typical states of super-repellant surfaces: ‘‘petal’’ state; ‘‘gecko’’ state; metastable Cassie state; liquid-infused state. Reproduced with permission from [55], Copyright 2007 John Wiley and Sons. Schematic illustration of the characterization analysis for contact angle hysteresis: (d) advancing θ_{Adv} and receding contact angle θ_{Rec}; tilt angle, i.e., the so-called roll off angle or sliding angle θ_{SA} (e) and the shedding angle θ_{SHA} (f). Reproduced with permission from [56], Copyright 2014 The Royal Society of Chemistry.

3.1.2. Contact angle hysteresis

A super-repellant surface requires not only the contact angle to be larger than 150° for water and oil droplets, but also corresponding low contact angle hysteresis (CAH). On a surface with a certain roughness or uneven chemical composition, two

contact angles, viz. the advancing contact angle (θ_{Adv}) and the receding contact angle (θ_{Rec}) can be measured, and their difference is defined as the CAH.[45] CAH affects the surface adhesion. For example, a low hysteresis is needed for a self-cleaning surface. Hence, CAH is another most significant character for superhydrophobic and superoleophobic surfaces. To date, lots of techniques have been developed for the characterization of the CAH, and among them $\theta_{Adv}/\theta_{Rec}$ and the tilt angle are most often employed.

Advancing/receding contact angle: Usually, a commercial instrument with an enhanced video microscopy system with the assistance of digital image analysis is applied to measure advancing contact angle (θ_{Adv}) and the receding contact angle (θ_{Rec}) (**Figure 3**d). Firstly, a standard water droplet is generated onto a substrate surface by a syringe pump. And then the water fluid is continuously pumped into (or sucked from) the droplet at a lower speed. Meanwhile, θ_{Adv} is displayed in a frame grabber by a solid state charge coupled device camera. Following the water pumping, the suction action is performed to recede the water droplet, and to record the θ_{Rec}.[57]

Tilt angle: A critical angle between the substrate and the horizontal surface is termed as the tilt angle, below which the droplet starts to move upon inclining the substrate. A tilt angle lower than 10^{o} for both water and oil droplets is believed to be necessary for the super-repellent surfaces and for self-cleaning performance. Usually, the tilt angle can be divided to two types, the sliding angle (θ_{SA}) (**Figure 3**e) and the shedding angle (θ_{SHA}) (**Figure 3**f). The sliding angle, namely roll-off angle, indicates the angle of inclination of a surface when a droplet completely rolls off the surface due solely to

gravity. The sliding angle is measured by the θ_{CA} measuring instrument with the assistance of a tilt plate possessing a tunable angle between 0° and 90°. During the measurement process, the plate keeps rotating from 0° to 90° until the droplet starts to slide away or roll off the substrate surface.[52, 58] Immediately the rotation angle is recorded as θ_{SA}. Strictly speaking, a slight distinction exists in sliding and rolling in terms of the actual motion of droplet. In comparison with the latter case, the contact area between the droplet and the substrate in sliding is slightly larger than rolling. In addition, the droplet is fixed on the substrate due to the high adhesive force in the former case while the droplet can roll freely in the latter case.[59-61] However, in most of the cases, the difference was not reported along with the recorded angle. When some rough substrates such as fabrics requires a measurement of surface adhesion, the sliding angle method is no longer applicable due to the numerous sticking fibers that interferes with the droplet sliding.[58] Therefore, for the characterization of superhydrophobic textile, a new approach known as shedding angle has been put forward.[62] Essentially, when a water droplet of defined volume dropped from a defined height start to bounce away or roll off the inclined substrate, the critical angle is defined as the shedding angle (θ_{SHA}). The measured θ_{SHA} value is affected by the drop volume and needle-to-substrate distance, therefore care has to be exercised when comparing measurements from different experiments.

3.2. The mechanism for superamphiphobicity

3.2.1. Chemical composition

The chemical composition plays a key role in the wettability of materials due to its determination on the surface energy. CA of a flat substrate is well described according to Young's equation (Equation 1).[4] To accomplish hydrophobicity or oleophobicity on a flat surface, the CA more than 90° for water and oil droplet is expected. If CA is larger than 90°, γ_{sv} is less thanγ_{sl}. Ignoring the actual order of the interaction force between two surfaces, we can approximate the γ_{sl} according to equation (4). [63]

$$\gamma_{sl} = \gamma_{sv} + \gamma_{lv} - 2\sqrt{\gamma_{sv}\gamma_{lv}}$$

(4)

By combining equation (1) and (2), it can be concluded that the surface free energy of the solid substrates (γ_{sv}) should be low enough to be smaller than one quarter of that of the liquid (γ_{lv}). Usually, the surface tensions of some typical oils, such as hexadecane at 27.5 m/Nm, are much lower than that of water. Hence, in order to realize superoleophobicity, the surface energy of the solid surface must possess very low surface energy with only a few m/Nm. This can only be achieved in virtue of some special molecular groups, such as -CF_3. This rigorous necessity features the difficulty in the fabrication of superamphiphobic surfaces and imposes restrictions on the selection of materials.

In general, the suitable materials for the effective construction of robust superamphiphobic coatings are mainly perfluoroalkanes and block-copolymers contain with a functional group at one terminal (F-monomer), such as, 1H,1H,2H,2H-perfluorooctyl phosphate (PFOP), 1H,1H,2H,2H-perfluorooctanoic

acid (PFOA), 1H,1H,2H,2H-perfluorooctyltrichlorosilane (PFOTS), 1H,1H,2H,2H-perfluorodecyltrichlorosilane (PFDTS), 1H,1H,2H,2H-perfluorodecane-1-thiol (PFDSH), and 1H,1H,2H,2H-perfluorodecyl acrylate (PFDAE). Moreover, it can also be realized by spray- or spin-coating a fluorinated-polymer (F-polymer) solution. Vapour or liquid phase deposition can also be usually applied to graft a fluorinated layer by using F-monomers.

3.2.2. Special rough morphology

Another vital factor is the surface topology. As described before, air can be trapped on a rough area when the liquids are brought into contact, thereby greatly reducing the contact between the surface and the droplets. However, only a certain type of rough structure with the re-entrant geometries is appropriate for constructing superoleophobicity, such as overhang structures, negative slopes, inverse-trapezoidal structures and mushroom-like structures (**Figure 4**d-g).[19, 30, 51, 64-73] As mentioned above, Tuteja et al. have firstly come up with the concept of re-entrant structure.[19] In their work, a kind of fiber mats was fabricated using a class of synthesized polyhedral oligomeric silsesquioxane (POSS) molecules. Although the CAs of the components were all smaller than 90°, the fiber mats exhibited superamphiphobic property due to the re-entrant structures. This means that in spite of a low CA on a flat surface (θ_{flat}), the CA on a practical rough surface can still be high enough in virtue of such structures. In **Figure 4**,[63] taking the surface with inverse-trapezoidal structures as an example, if the summation of the re-entrant geometric angle of this texture (α) and contact angle on a flat surface (θ_{flat}) is larger than 90°, a favorable shape can be

supported by such geometry on the liquid-vapor interface and the surface tension is directed upward. The surface with this structure is not wetted by the liquid due to the air pockets and the low contact fraction of the composite liquid-solid. As displayed in **Figure 4**b, various liquids can display high CAs on the surfaces with structures of re-entrant curvature even if the contact angles on a flat surface are lower than 90°. Hence, liquids with various flat contact angles can wet the re-entrant curvature to different extents to achieve a favorable liquid-vapor interface shape. In addition, bringing in the re-entrant surface curvature will not only strengthen the stability of the superamphiphobic surface but also facilitate the choice of corresponding oleophilic materials for preparing superamphiphobicity. In general, to successfully achieve superamphiphobicity, the aforementioned two parameters should be taken into consideration complementarily and comprehensively.

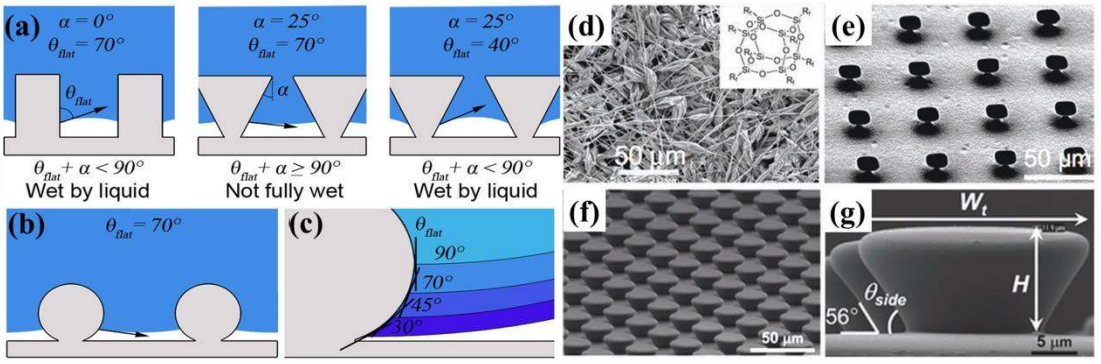

Figure 4. (a) θ_{flat} angles of < 90° on non-re-entrant and re-entrant geometries, liquid does not fully wet structure if $\theta_{flat} + \alpha \geq 90°$ thanks to favorable shape of the liquid-vapor interface, (b) geometry with re-entrant curvature supporting a θ_{flat} angle 70°, (c) geometry with re-entrant curvature supporting various θ_{flat} angles of ≤ 90°. Reproduced with permission from [63]. Copyright 2016 Wiley. (d,e) SEM images of electrospun fluorodecyl POSS surface and microhoodoo surface. The insert shows the

molecule structure of fluorodecyl POSS molecules. Reproduced with permission from[51]. Copyright 2008 The National Academy of Sciences of the USA. (f,g) SEM images of PDMS surface with inverse-trapezoidal microstructures array. Reproduced with permission from [30]. Copyright 2010 The Royal Society of Chemistry.

4. Fabrication methods for superamphiphobicity

Herein, we will make a summary of the fabrication methods for the superamphiphobic substrates. To best of our knowledge, the appropriate union of rough surface structure and surface chemical composition is considered to make significant contribution for constructing super-antiwetting surfaces. Hence, two basic procedures are always involved in the preparation process, viz. to form the nano/micro-scale roughness on the surface and to modify the surface by some materials with low surface energy. According to the operation order of these two steps on the substrates, the construction strategies can be classified into the following three types (**Figure 5**): (1) the 'pre-texturing + post-modifying'; (2) the 'pre-modifying + post-texturing'; (3) incorporating surface roughness with surface modification in one step, viz. in-situ construction strategy.

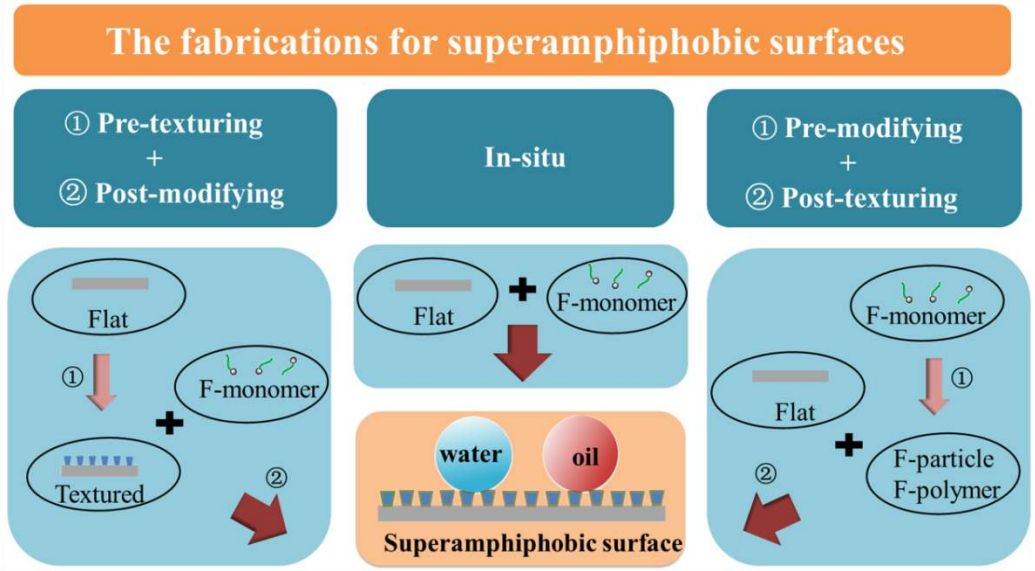

Figure 5. Three types of construction strategies for superamphiphobic surfaces.

4.1. 'Pre-texturing + post-modifying' strategy

4.1.1. Dip-coating

As one of the most convenient techniques, dip-coating has been employed to fabricate super-repellent surfaces with assistance of some micro- or nano-particles to form rough structures.[74-81] Lin and his coworkers [79] have reported that the fabrics after a two-step dip-coating technique with hydrophobic nanoparticles and FAS/FD-POSS (fluoroalkyl silane/fluorinated-decyl polyhedral oligomeric silsequioxane) were endowed with outstanding superamphiphobic property and exceptional multi-self-healing ability against physical and chemical damages (**Figure 6**a-g). The prepared coating has demonstrated its durability to resist 5000 cycles of Martindale abrasion and 200 cycles of laundrying without an obvious change in the superamphiphobicity. This group of authors have also applied another new coating system consisting of poly(vinylidene fluoride-co-hexafluoropropylene), fluoroalkyl

silane, and modified silica nanoparticles to obtain a durable self-healing superamphiphobic surface which can withstand at least 8000 cycles of abrasion and 600 cycles of standard laundrying.[80] These simple but novel and effective coating systems are useful for the development of robust protective clothing for various applications only via a facile dip-coating method. On basis of a mussel-inspired dendritic polymer (MI-dPG) coating with precisely controllable roughness, Schlaich et al.[81] have described an efficient and facile dip-coating approach to achieve highly hierarchical surface coatings with superamphiphobicity either directly by pH-controlled aggregation or in combination with nanoparticles (NP). By simply adjusting the depth of the coating solution, the thickness and roughness gradient of coatings was possibly fabricated (**Figure 6**h-o). Geng et al.[74] have firstly combined silica nanoparticles including solid silica nanoparticles (ca. 20 nm) and hollow silica nanoparticles (ca. 60 nm) with an acid-catalyzed silica sol as a binder solution to construct superamphiphobic coatings with robust durability and highly transparency via dip-coating and subsequent spray-coating.

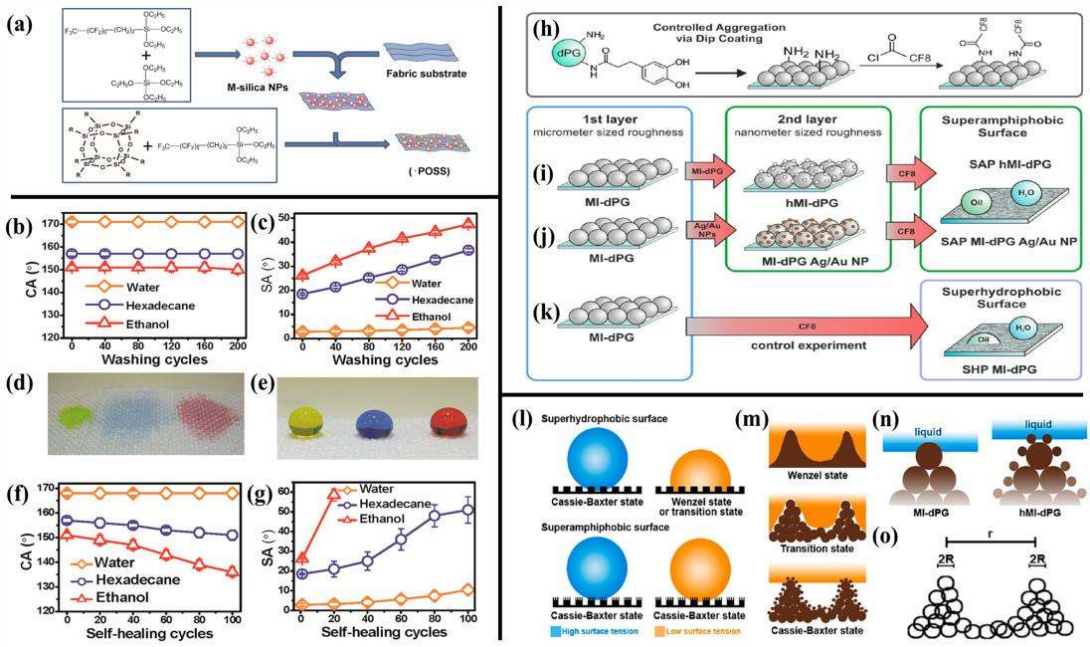

Figure 6. (a) Chemical structures of coating materials and procedure for coating treatment; (b) SEM images of coated polyester fibers; (b) CA and (c) SA versus washing cycles, (d,e) photos of water, hexadecane, and ethanol drops on the coated fabric (d) after plasma treatment and (e) the plasma treated fabric after heating at 140°C for 5 min. (f,g) Effect of plasma and self-healing cycles on CA and SA of the FS-NP/FD-POSS/FAS coated fabric (here one "plasma and self-healing cycle" is defined as 5 min plasma treatment followed by 5 min heating at 140°C). Reproduced with permission from [79]. Copyright 2013 American Chemical Society. General coating approach. (h) Left: Structure of the mussel-inspired dendritic polyglycerol (MI-dPG); Right: Resulting MI-dPG coating and post-modification with heptadeca-fluoroundecanoyl chloride (CF8); Fabrication approach of (i) Quasi-superamphiphobic hierarchical MI-dPG surface coatings (SAP hMI-dPG), (j) Quasi-superamphiphobic MI-dPG with Ag/Au NPs surface coatings (SAP hMI-dPG), and (k) Micro-roughened, superhydrophobic MI-dPG (SHP MI-dPG) coating.

Different states of antiwetting. (l) The liquids with low surface tension cause the transition from the Cassie−Baxter state to the Wenzel state on MI-dPG superhydrophobic surfaces but not on hMI-dPG quasi-superamphiphobic surfaces. (m) Different wetting models: Wenzel mode (wetting state), Cassie−Baxter-to-Wenzel transition state, and Cassie−Baxter mode (lotus state). (n) Hierarchical structure of the hMI-dPG surfaces decreased the area fraction of the projected liquid−solid interface. (o) Schematic of structure features. Reproduced with permission from [81]. Copyright 2016 American Chemical Society.

4.1.2. Photolithography

Particularly, taking advantage of precise control of photolithography technology on the substrates, this method can be used to fabricate patterned surfaces with various sizes and shapes. In addition, because of easily fabricated template and reusability, this technique can be made economical for various regular structures.[25, 30-32, 82-88]

In Zhao's group,[25, 31, 87] various well-organized structures, including pillars with wavy side walls (**Figure 7**d), straight smooth side walls (**Figure 7**e), overhang re-entrant structures (**Figure 7**f) and grooved textures (**Figure 7**g) were prepared on a silicon wafer via a facile photolithography technology under an already prepared mask to transfer these patterns to the wafers. Similarly, a perfectly ordered inverse-trapezoidal array was constructed on a flexible transparent PDMS surface via the backside 3-D diffuser lithography and the subsequent PDMS replication processes.

In another work, photoresist micropillars decorated with nanoparticles of the

same photoresist are produced with a hierarchical design derived from common photolithography incorporated with spontaneous emulsification by Li et al,[32] leading to the formation of a convex and re-entrant structure. The strong chemical bonding between the micropillars and the nanoparticles has endowed the coated surface with robustness and durability (**Figure 7**a-c). Coincidentally, Darmanin et al.[88] have combined lithography with electropolymerization to fabricate the similar morphology and structure. Micro-patterned surface with cylindrical arrays was prepared with lithography, followed by electropolymerization of a fluorinated polymer.

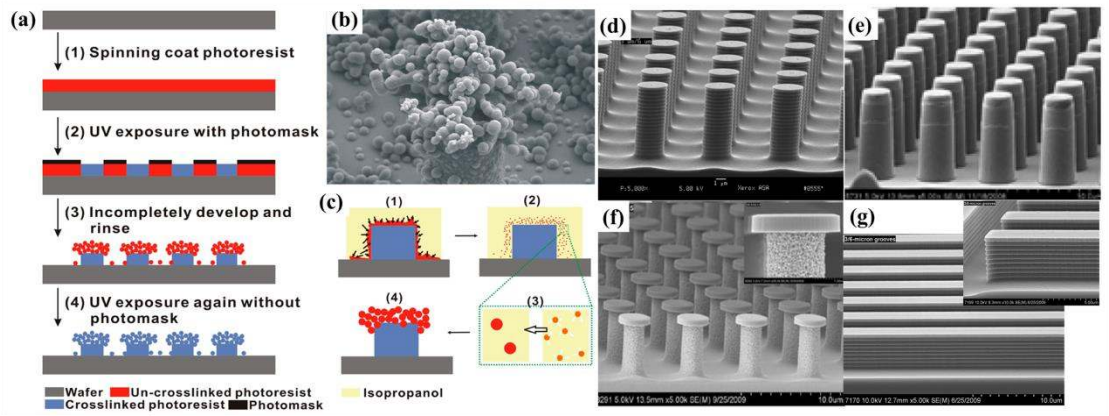

Figure 7. Schematic illustration of one-step photolithography process for engineering superamphiphobicity. (a) Process for the fabrication of micropillars decorated with nanoparticles to achieve superamphiphobicity. (b) SEM image of the nanoparticles' inlaid micropillar (6 μm in diameter). (c) Schematic showing the formation of nanoparticles by the "Ouzo effect", where (1) isopropanol diffuses into the residual un-cross-linked SU-8 solution in developer; (2) supersaturation of the SU-8 causes homogeneous nanometric size droplets; (3) diffusion of SU-8 into nearby droplets forms bigger droplets; (4) SU-8 droplets attach to pillars after isopropanol is removed. Reproduced with permission from [32]. Copyright 2015 American Chemical Society.

Well-defined structures prepared via Lithography. (d) pillars with wavy side walls. Reproduced with permission from [87]. Copyright 2012 American Chemical Society. (e) straight smooth side walls. (f) overhang re-entrant structures. Reproduced with permission from [31]. Copyright 2012 American Chemical Society. (g) grooved textures. Reproduced with permission from [25]. Copyright 2012 American Chemical Society.

4.1.3. Etching

As a facile and inexpensive technique, etching can be applied to create surface rough texture. On basis of whether solutions are used or not, etching techniques can be classified into dry etching and wet etching. In common, some simple equipments are suitable for wet etching method. However, it is difficult to control the surface morphology very well, especially for miniature materials. In comparison, dry etching can be easily controlled without any residues from the solution. However, the disadvantage is that more complicated and costly equipment is usually required.

Using some polymeric substrates such as polydimethylsiloxane (PDMS), polyether ether ketone (PEEK) and polymethyl methacrylate (PMMA), Kosmas et al.[89] firstly constructed hierarchical micro-nanotexture on these surfaces by combining plasma etching with grafting of perfluorinated monolayer (**Figure 8**a-c). In terms of cellulose-based substrates such as paper, Li et al.[90] have presented a similar method to fabricate superamphiphobic paper surfaces via a fluoropolymer deposition. The heterogeneous morphology of paper thoroughly differs from that of those artificial superamphiphobic surfaces. After above two steps, the refined wood fibers

with smaller size are formed to hold various droplets.

Some engineering metals and alloys can be roughed by solution etching. Peng et al.[91] have prepared flowerlike morphology on aluminum surfaces by a simple chemical etching with HCl solution and immersion process in boiling water (**Figure 8**f). In addition, Li et al.[92] constructed superamphiphobic hierarchical bimetallic micro/nanostructures with labyrinth-like concave-convex microstructures and dendritic Ag nanostructures on Al alloys surfaces by immersing the etched sample into $AgNO_3$ solution for the Ag deposition. Wang et al.[93] have combined H_2O_2 and HCl (or HNO_3) to construct hierarchical structures on steel, followed by a surface modification treatment (**Figure 8**d,e). Dual geometric architectures with micro/nano-structures has been obtained by Sumit et al.[94] via a combination of simple chemical etching with HCl solution and subsequent anodization in H_2SO_4 solution (**Figure 8**g).

Besides the aforementioned etching methods, some other etching techniques, for example, electrochemical etching, ion etching and so on, can also be employed on basis of the different chemical nature of the substrates.

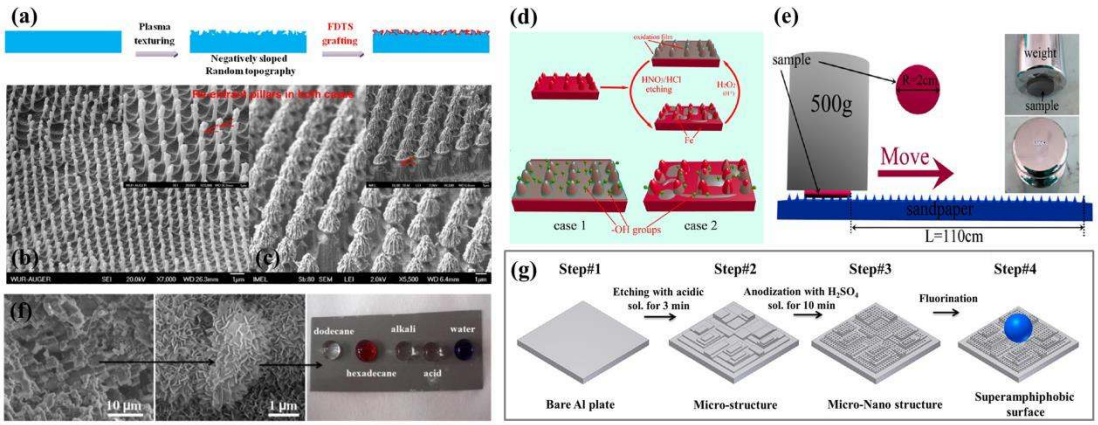

Figure 8. (a) Two-step approach to obtain superamphiphobic surfaces via

plasma-induced texturing and follow-up reaction with FDTS ($Cl_3SiCH_2CH_2$-$C_{10}F_{21}$). SEM images of PMMA surfaces (60° tilted) displaying the hierarchical, hexagonally ordered packed pillars obtained upon plasma etching using (b) 1 μm and (c) 3 μm polystyrene particles. Reproduced with permission from[89]. Copyright 2014 American Chemical Society. (d) Schematic view of the reacting process and surface hydroxyl on the oxidation surface before and after the chemical etching. (e) Illustration of the abrasion test for A6 surface at 500 g loading on sandpaper (400 grid SiC). Reproduced with permission from[93]. Copyright 2015 American Chemical Society. (f) Low- and high-magnification FESEM images of the surface after etching in a HCl solution for 8 min and immersion in boiling water for 15 min (MNS-surface) and Various droplets staying in spherical shapes on the treated surface. Reproduced with permission from[91]. Copyright 2014 American Chemical Society. (g) The fabrication process of dual geometric architectures with micro- and nanoscale structures on the surface of the Al plate. Reproduced with permission from[94]. Copyright 2013 American Chemical Society.

4.1.4. Thermal reaction

Thermal reaction, including hydrothermal method and solvothermal method, is another utile method to construct rough structure with uniform dispersity and high purity. And the surface morphology can be well controlled by dissolving substance surface under combined temperature and pressure conditions.[95-101] However, the required operational conditions may pose challenges to the production cost and scalability. Recently, a flower-like superamphiphobic FOTS-TiO_2 powder was

synthesized by Chen et al.[99] via solvothermal reaction and subsequent functionalization treatment. The FOTS-TiO_2 powder possesses a similar surface morphology to the lotus leaf with hierarchical micro/nanostructures (**Figure 9**a-d). However, it has a more attractive property of superoleophobicity beyond the lotus leaf. Additionally, Yu et al.[100] have studied pompon-like and chip-like $FeSe_2$ particles by a one-step solvothermal reaction with the assistance of hydrofluoric acid (HF) for the first time. HF in this work played a significant role in controlling the morphology of the $FeSe_2$ particles (**Figure 9**e-j). A simple hydrothermal process was employed by Gao et al. to fabricate durable superamphiphobic films of cuprous oxide (Cu_2O) microspheres on a wood substrate.[101]

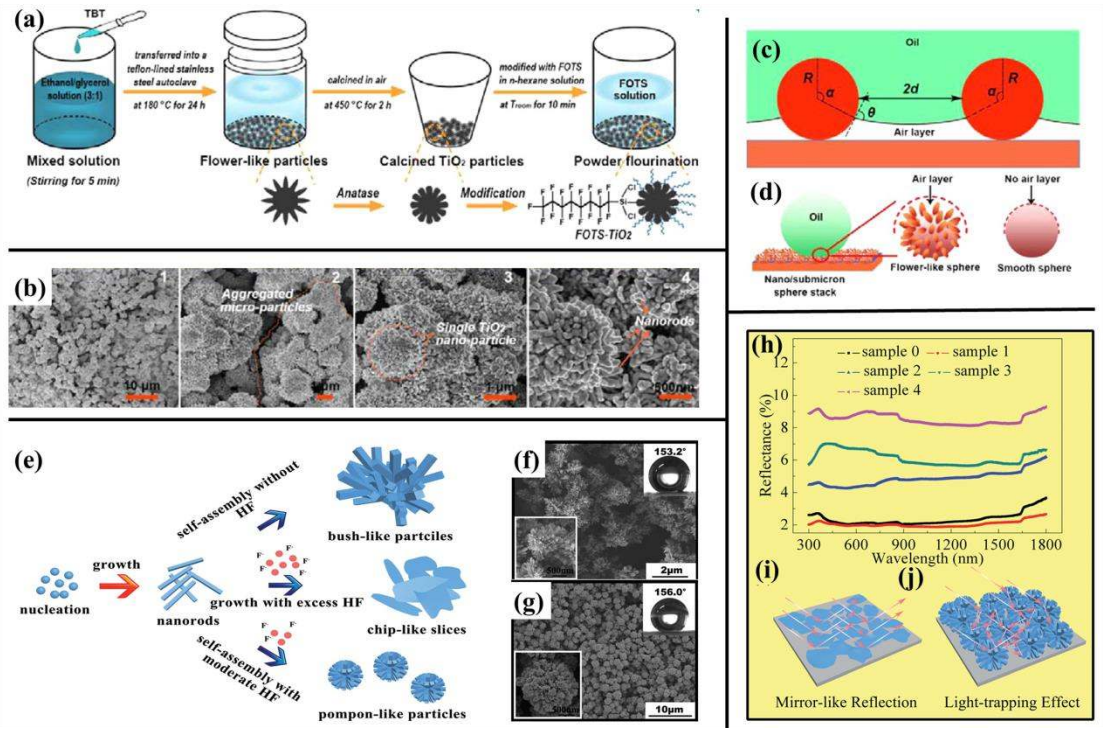

Figure 9. (a) Schematic of preparing flower-like superamphiphobic FOTS-TiO_2 particles; (b) Top-view SEM images of coated glass slide, showing multilevel microaggregates/submicro-particles/nanorods structures. (c) Schematic illustration of

oil droplet sitting on the top layer of smooth-particle-based coating, highlighting the re-entrant structure and expected liquid-vapor interface[a]; (d) Schematic diagram for oil droplet sat on two types of TiO_2 sphere stacking layers: Hierarchical flower-like sphere and smooth sphere. ([a]R and d are the radius and spacing of particles, respectively). Reproduced with permission from [99]. Copyright 2016 American Chemical Society. (e) The schematic illustration of the morphological changes with dosages of HF. (f) and (g) are the SEM images of samples before and after the addition of HF, respectively; insets in the bottom left corners of (f) and (g) are the corresponding magnified images. (h) Diffuse reflectance of different samples with wavelength ranging from 300 nm to 1800 nm. (i) and (j) show two different reflection schematics of $FeSe_2$. Reproduced with permission from [100]. Copyright 2014 The Royal Society of Chemistry.

4.1.5. Chemical vapor deposition

Chemical vapor deposition (CVD) is a facile method for the deposition of superhydrophobic materials by surface reaction of gas phases.[102-104] CVD technique can be applied in many forms, each of which possesses its own specific routes. Maximeet al.[105] have introduced a soot-templated silica surface by a CVD technique. The prepared surface was fractal like, highly porous, repellent to liquids. As we all know, soot is composed of many carbon nanoparticles with a diameter of about 40 nm in a highly porous network. Van der Waals forces are considered to exist to connect these nanoparticles loosely and the particles agglomerate into strings. The obtained network was fragile and unstable, and it was then stabilized by depositing TEOS via

CVD to form a silica shell referred as coated soot **(Figure 10**a,b,c). In another work by Li et al., a kind of microscale porous structure was also fabricated by combining ice templation with CVD using dopamine and fumed SiO_2 nanoparticles as initial building blocks.[106] In terms of the excellent adhesive ability of polydopamine, the obtained superamphiphobic coatings have been employed to various substrates successfully including natural and artificial materials (**Figure 10**d,e,f,g).

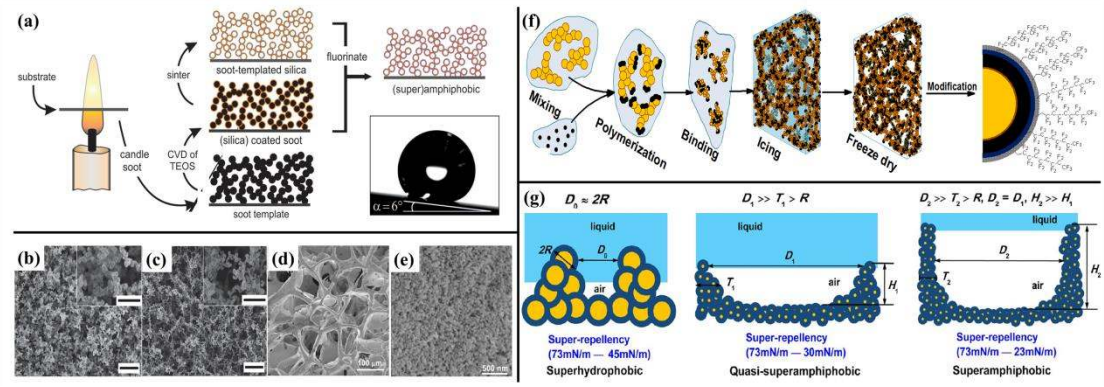

Figure 10. (a) Scheme of sample preparation: Collection of candle soot on the substrate. Silica is deposited by CVD of TEOS. Afterwards, the coated soot was sintered at various temperatures. Deposition of a fluorosilane by CVD made the surfaces liquid repellent. SEM images of soot-templated surfaces exposed to different periods of CVD and sintering temperatures, (b) coated soot exposed to 24 h CVD, (c) soot-templated silica sintered at 600°C, The scale bars are 2 µm and 500 nm (inset). Reproduced with permission from [105]. Copyright 2016 Wiley. SEM images of (d) superficial layer and (e) inside layer of the microscale porous structure. (f) Schematic depicting of the formation of the porous structure and further surface fluoroalkylsilanization to the porous structure. Yellow clusters denote the branched hydrophilic fumed silica nanoparticles. Separated black circles denote dopamine

molecules. Connected black circles denote polydopamine molecules. (g) Schematic illustration for structure features of nanoscale porous superhydrophobic coating, thin microscale porous quasi-superamphiphobic coating, and thick microscale porous superamphiphobic coating. In the three images, the nanoparticle diameters are all 2R. Reproduced with permission from [106]. Copyright 2016 American Chemical Society.

4.1.6. Electrospinning

As a versatile and scalable technique, electrospinning is applicable to produce micro/ nanoscale fibers with various polymers.[107-113] As a laboratorial experiment, it needs a high-power supply, a syringe pump, a conducting collector, and a polymer with high molecular weight. Between a syringe nozzle and a conducting collector, an electrical potential is applied to form a high electric field to initiate the electrospinning process. Generally, the polymer solution was extruded to form a charged liquid jet from the tip of a distorted droplet for the reason that the surface tension is overcome by electrostatic repulsion between the charges due to the high electrical potential. After experiencing whipping and bending instabilities from the syringe nozzle to conducting collector, the liquid jet has enough time to make its solvent to completely evaporate and deposit on the collector, ultimately forming a solid fiber membrane.

In recent study, electrospinning has been employed to prepare superamphiphobic surfaces using common or fluorinated polymers. Ganesh et al.[114] have prepared rice-shaped TiO_2 nanostructures to create a robust superamphiphobic coating on glass substrates via electrospinning technique followed by sintering and silanization

(**Figure 11**a-f). The obtained coating displayed robust mechanical and thermal stability with strong adhesion to the glass substrate, thus paving way for the prospective applications in a large scale. In addition, their group has also electrospun SiO_2 nanofibers with one-dimensional morphology used as a template, and then deposited a super-thin layer of porous SiO_2 membrane by CVD technique. The obtained superamphiphobic coating was robust and transparent. The fiber morphology assisting the hybrid SiO_2 network was considered to contribute to the surface texture and the roughness. In another work by Pan et al.,[115] they have fabricated surfaces with hierarchical structure using electrospinning technique with blend solution of cross-linked poly(dimethylsiloxane) + 50% FD-POSS (w/w) on the stainless steel wire meshes (**Figure 11**g-k). The re-entrant curvature can be observed on such surface at the coarser and finer length scale. The prepared coating possesses low surface energy and a re-entrant curvature, which have contributed to superamphiphobicity towards a wide range of Newtonian liquids with diverse low surface tensions such as a variety of acids, alkalis, and solvents.

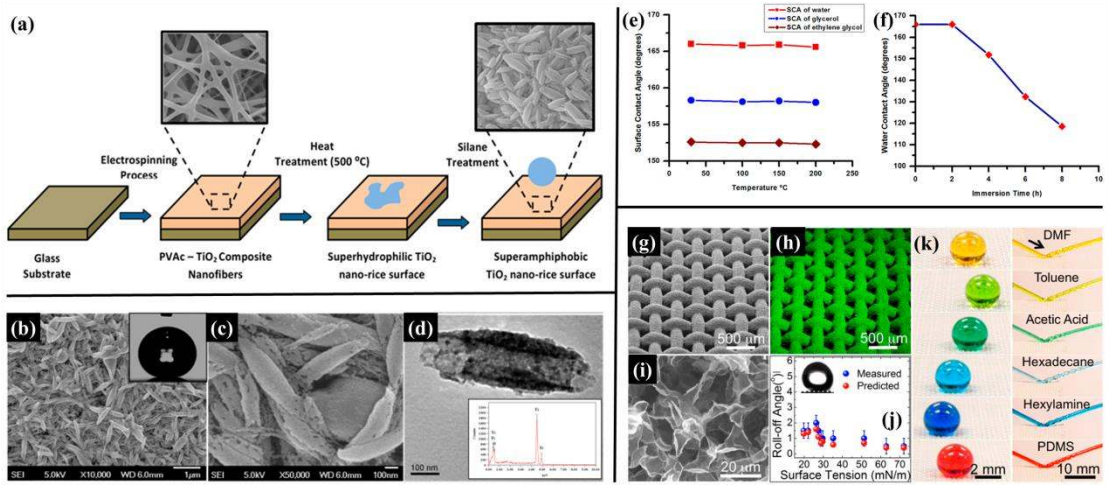

Figure 11. (a) Fabrication of superamphiphobic coating: process flow chart (this

schematic is not drawn to scale); (b, c) SEM images (low and high magnification) of the TiO_2-coated samples (inset: interaction of water droplet (1 μL) with the coated surface. WCA: 166°); (d) TEM image of a single nano-rice structure (inset: EDS spectrum of the TiO_2 coated sample); (e) Surface contact angle values made by water, glycerol and ethylene glycol droplets on the superamphiphobic surface after heat treatment for 2 h at different temperatures; (f) WCA values made by the water droplets on the TiO_2-coated surface for different immersion time in hot aqueous ethanol solution. Reproduced with permission from [114]. Copyright 2013 American Chemical Society. (g) SEM image of the hierarchically structured surface illustrating the electrospun coating of cross-linked PDMS + 50 wt.% fluorodecyl POSS on a stainless steel wire mesh 70. (h) Elemental mapping of fluorine on the hierarchically structured surface. The high surface fluorine content is expected to be due to the surface migration of the fluorodecyl POSS molecules. (i) SEM image illustrating the reentrant curvature of the electrospun texture. (j) Roll-off angles for various Newtonian liquids on the surface shown in (g). The inset shows an ethanol droplet rolling on the surface at a roll-off angle of 2°. (k) Droplets of various low surface tension Newtonian liquids showing very high contact angles on the surface and the jets of different Newtonian liquids bouncing on the surface. Reproduced with permission from [115]. Copyright 2012 American Chemical Society.

4.2. Pre-modifying + post-texturing strategy

4.2.1. Spray-coating

For a spray process, a spray gun with an air pump is sufficient. There is no reliance of complex facility setup, complicated operation process, and various restrictions on the substrates to be used. With regard to such a common and facile method, fluorinated nanoparticles or polymers have to be prepared in advance, and subsequently sprayed on flat substrates, thereby generating roughened layer with low surface energy on the surfaces.[116-122] Ge et al.[119] have prepared a separator by spraying fluorinated silica nanoparticles (NPs) on a paper towel to form a superamphiphobic surface. By going through a two-step pre-wetting procedure, the obtained paper towel can be used to selectively separate water or oil from the mixture (**Figure 12**a-c). Different from the previously reported methods, Dong et al.[120] have constructed the micro- or nano-structure of the superamphiphobic coatings by using the abundant natural PAL nanorods as the building blocks via a simple spray-coating method. The developed process ensured possibility of large-scale production for a wide range of practical applications (**Figure 12**d-g). Subsequently in recent work, this research group has also applied a spray-coating method to prepare the robust transparent superamphiphobic surfaces using the homogeneous suspension of polysiloxane-modified multi-walled carbon nanotubes (MWCNTs@POS) on glass substrates, followed by annealing in air to obtain the silica nanotubes (SNTs). The obtained superamphiphobic surfaces displayed extremely high contact angles and low sliding angles towards a variety of liquids with diverse surface tensions.[121] Besides theses nanoparticles and other nanostructures, Srinivasan et al.[122] have constructed the re-entrant structure by spraying polymer-based coating consisting of the hybrids

of 1H,1H,2H,2H-heptadecafluorodecyl polyhedral oligomeric silsesquioxane (fluorodecyl POSS) and poly(methyl methacrylate) (PMMA). By systematically varying the molecular weight and component concentration of the polymer solution, the surface morphology can range from a randomly corpuscular or spherical microstructure to a beads-on-string structure and even to bundled fibers.

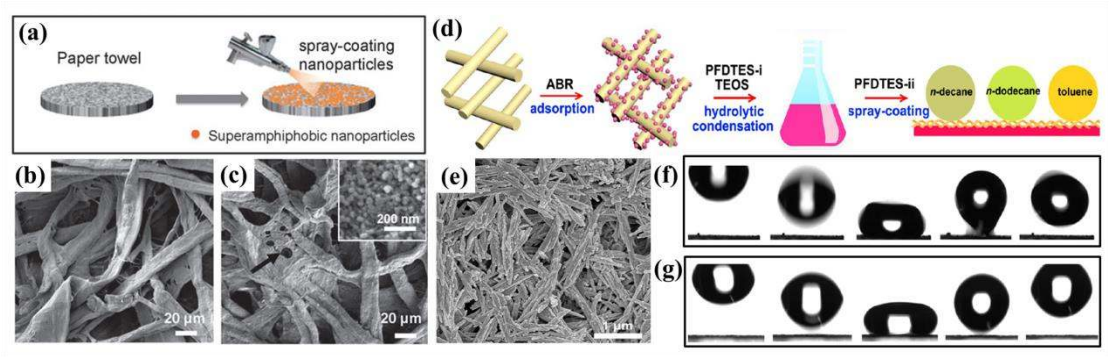

Figure 12. Schematic illustration of (a) the preparation of superamphiphobic paper. SEM images of (b) pristine paper towel and (c) SA-paper. Inset: the assembly of stringed fluorinated NPs on cellulose fiber. Reproduced with permission from [119]. Copyright 2015 The Royal Society of Chemistry. (d) Schematic illustration for preparation of the superamphiphobic PAL/ABR @ fluoroPOS coatings. (e) SEM image of the PAL/ABR@fluoroPOS coating with a $CPFDTES_{-ii}$ of 7.6 mM. Bounce behaviors of (f) n-decane and (g) water droplets on the PAL/ABR@fluoroPOS coating. Reproduced with permission from [120]. Copyright 2016 American Chemical Society.

4.2.2. Grafting

Xiong et al.[123] have synthesized a new diblock copolymer, poly[3-(triisopropyloxysilyl)propyl methacrylate]-block-poly[2-(perfluorooctyl)ethyl methacrylate] (P1 or PIPSMA- b-PFOEMA), that bore a fluorinated PFOEMA block

and a sol-gel forming PIPSMA block via sequential anionic polymerization, which was then grafted onto silica particles. The obtained superamphiphobic paper coated with P1-grafted SiO_2 particles exhibited high CAs towards water and even the cooking oil droplets (**Figure 13**d,e). Similarly, a novel report by Zhang et al.[124] has demonstrated a "grafting from" method to synthesize copolymer-bearing silica particles based on the growth of bifunctional random copolymers on the silica particles via atom transfer radical polymerization (ATRP). The obtained superamphiphobic coating was so durable that it could withstand both NaOH etching and solvent extraction because of the strong covalent binding of the copolymer-functionalized SiO_2 with each other and to the substrates, which can be applied onto various substrates with hydroxyl-group like glass, wood and cotton (**Figure 13**a,b).

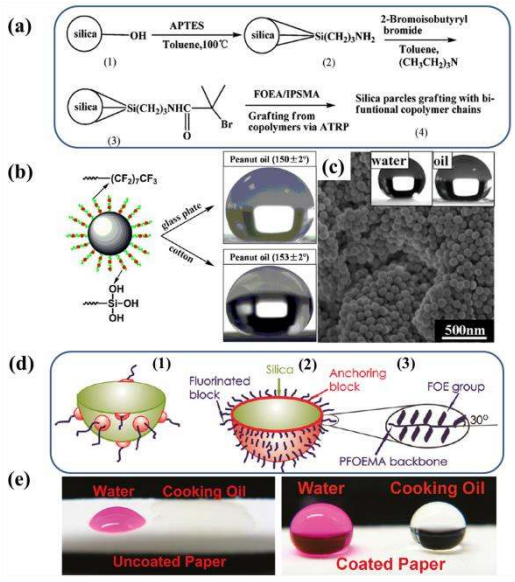

Figure 13. (a) Synthetic route for modifying silica particles and subsequently growing bifunctional copolymer chains from the modified silica particles. Amino group-bearing silica particles were prepared via reaction with APTES (1→2) before

an initiator was introduced onto the surfaces of these particles (2→3). Subsequently, bifunctional random copolymer chains were grown from these initiator-bearing particles via ATRP via a "grafting from" approach (3→4). (b) the growth of bifunctional random copolymer chains from silica particles through a "grafting from" approach and the use of these copolymer-bearing particles to fabricate superamphiphobic coatings. (c) SEM images of a PS-coated glass plate. Reproduced with permission from [124]. Copyright 2013 American Chemical Society. (d) Schematic Structures of P1-Grafted Silica Particles Prepared at Low (1) and High (2) P1-to-SiO_2 Mass Feed Ratios and the Packing of the Rodlike Perfluorooctylethyl (FOE) Groups and the PFOEMA Backbone at High P1 Grafting Densities (3). (e) Photograph of cooking oil and water droplets on the surfaces of uncoated (left) and coated (right) printing paper. Reproduced with permission from [123]. Copyright 2011 American Chemical Society.

4.3. In-situ construction

In contrast to the aforementioned two strategies, a one-pot method is deemed to be simpler for the fabrication and thereby has frequently been studied.[107, 125-135] Recently Lin et al. applied an in situ one-step vapour phase polymerization method to prepare electrically conductive superamphiphobic fabrics with polypyrrole in conjunction with fluorinated alkylsilane.[130] Subsequently, 3,4-ethylenedioxythiophene uniting with FD-POSS and 1H,1H,2H,2H-perfluorooctyltriethoxysilane (FAS) was employed to construct a

robust superamphiphobic surface with electrical conductivity by a one-step vapour-phase polymerization method.[131] The combination of FAS with FD-POSS played a key role in greatly improving the mechanical stability while showing a slight effect on the conductive ability. After more than 10000 cycles of the abrasion and 500 cycles of standard laundry test, almost no apparent change on superamphiphobicity of the obtained fabrics and the conductivity only displayed a very slight reduction. Moreover, the prepared surface showed self-healing properties. The superamphiphobicity could automatically recover from chemical damage completely, which is very useful for practical use (**Figure 14**).

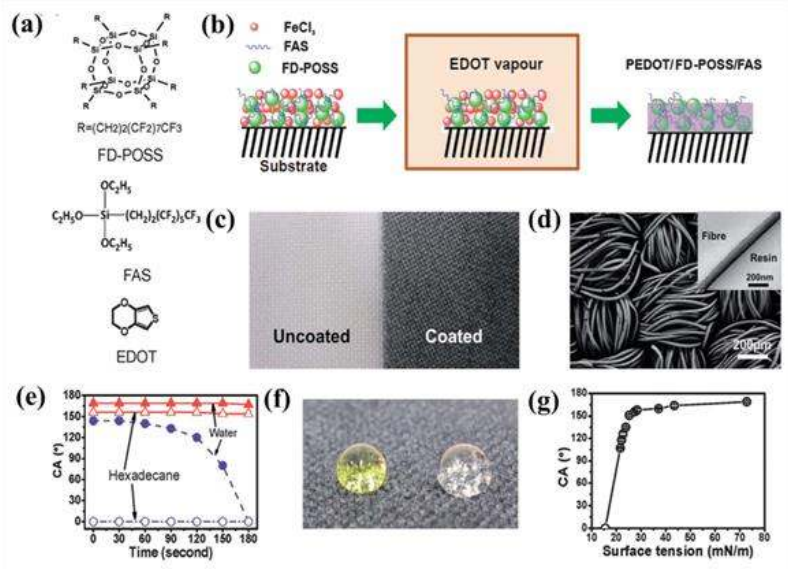

Figure 14. (a) Chemical structures of FD-POSS, FAS and EDOT, (b) illustration of vapour-phase polymerization to form PEDOT/FD-POSS/FAS coating on fabrics, (c) photo of polyester fabric before (left) and after (right) coating treatment, (d) SEM image of the polyester fabric after coating with PEDOT/FD-POSS/FAS (inset is a cross-sectional TEM image of a PEDOT/FD-POSS/FAS coated fibre), (e) contact angle of the coated fabric changing over time from initial fluid–fabric contact, (f)

coloured water (yellow) and clear hexadecane drops on the PEDOT/FD-POSS/FAS coated fabric, (g) dependency of the contact angle on the surface tension of fluids. Reproduced with permission from [131]. Copyright 2013 The Royal Society of Chemistry.

In Jiang and his co-worker's work,[132] a one-step electrodeposition method was developed to fabricate superhydrophobic coating on a variety of electrically conductive substrates and n-tetradecanoic acid was selected as an electrolyte. The obtained coating with hierarchical micro/nano-scale morphology showed outstanding super-repellency to various corrosive liquids at different pH values, such as acid, salt and basic solutions. By applying nonadecafluorodecanoic acid instead of n-tetradecanoic acid, superamphiphobic coatings were successfully prepared with a flowerlike microcluster morphology consisting of nanosheets. The synergy effect of their unique surface structures and chemical compositions has endowed the obtained surface with superamphiphobicity.[133] In contrast to the utilization of multi-step processes to construct superamphiphobic surfaces, such one-step construction strategy is simpler and more convenient.

Pereira et al.[134] have in situ synthesized mesoporous silica nanoparticles (MSNs) functionalized with tridecafluorooctyltriethoxysilane (F13) on the cotton fabrics via a one-pot co-condensation method (**Figure 15**). Hexadecyltrimethylammonium chloride (CTAC) and triethanolamine were chosen as the template and base, respectively. Such one-pot co-condensation method in this work provided the construction of novel multifunctional composite materials with a facile, efficient and

time-saving route.

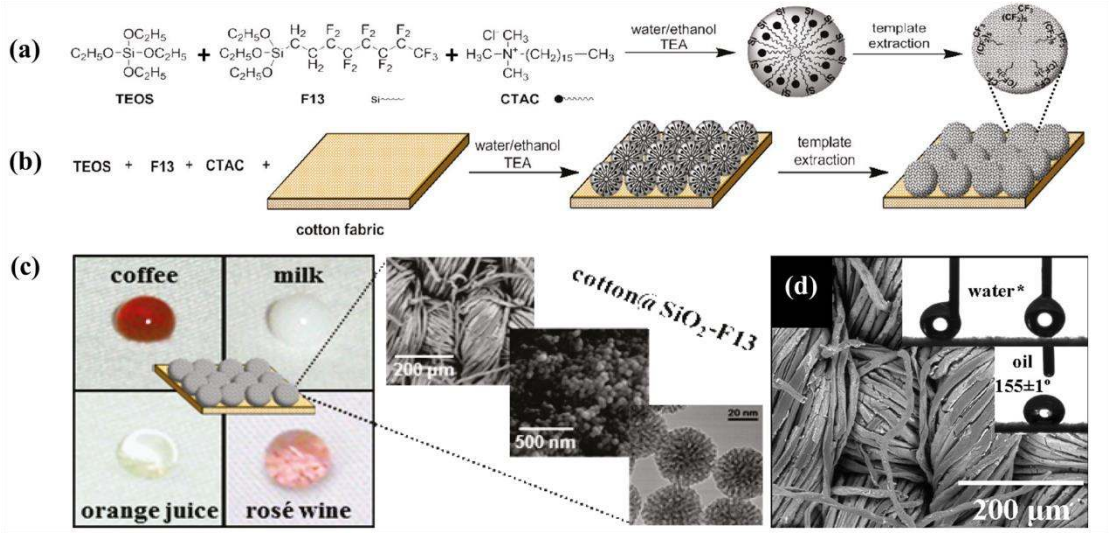

Figure 15. Schematic representation (not drawn to scale) of: (a) Synthesis of F13-MSNs and (b) Fabrication of hybrid cotton textiles functionalized with F13-MSNs, by one-pot co-condensation methodologies; (c) Various droplets stayed in a spherical shape on the SiO_2-F13@cotton surface; (d) SEM micrographs of cot@F13_1:5, photographs of water and oil droplets on the surface of the hybrid fabrics and CA values. Reproduced with permission from [134]. Copyright 2011 American Chemical Society.

Additionally, a facile one-step i-CVD route has been developed by Kim et al. to fabricate a robust superamphiphobic coating on a sponge surface, in which no additional solvent was required, thereby resulting in an all-dry vapor-phase process.[135] By such a single simple step of the i-CVD process, the poly(3,3,4,4,5,5,6,6,7,7,8,8,9,9,10,10,10-heptadecafluorodecyl methacrylate) (PFDMA) was successfully deposited onto both the interior and exterior of the sponge structure relying on the polymerization of fluoroalkyl acrylates (**Figure 16**). Furthermore, a room temperature condition is sufficient for the i-CVD process,

thereby contributing to its application on a variety of vulnerable substrates such as cellulose-based materials, which otherwise may be easily damaged by heating.

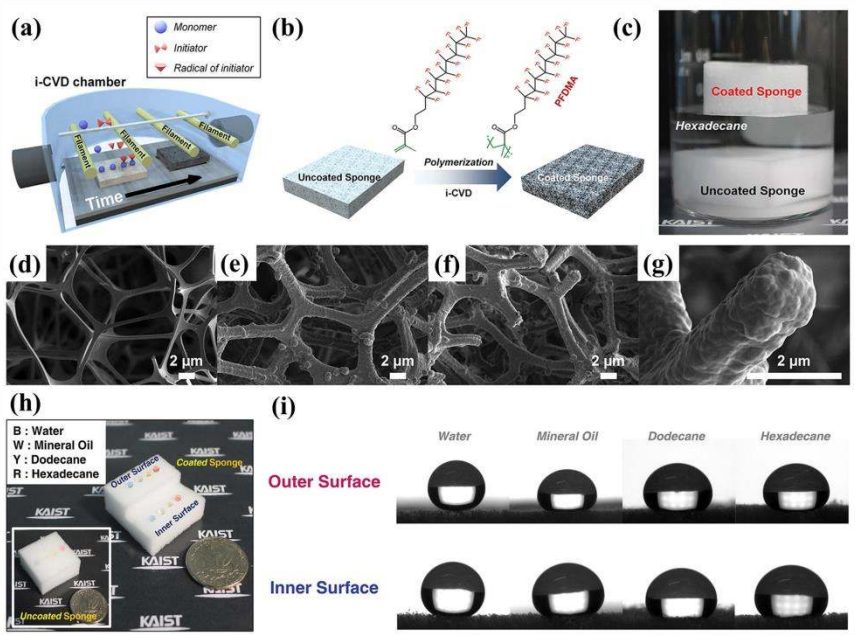

Figure 16. (a) Schematic illustration of the i-CVD process for SA-sponge fabrication. (b) Reaction scheme for polymerization of fluoroalkyl acrylates by the i-CVD process. (c) Digital camera snapshot of the SA-sponge and bare sponge submerged in hexadecane solvent. Morphologies of (d) skeleton in bare sponge, (e) skeleton in outside of the SA-sponge, (f) skeleton in inside of the SA-sponge, and (g) skeleton of the SA-sponge at high resolution using SEM. All scale bars are 2 μm. (h) Snapshot of various liquid droplets on the SA-sponge. The inset image shows the same liquid droplets on the bare sponge. (i) Photographs of contact angles of aforementioned liquid droplets on the inside and outside surface of the SA-sponge. All the contact angles exceed 150°. Reproduced with permission from [135]. Copyright 2016 Nature.

In another work,[107] Han et al. have prepared a kind of core-sheath-structured nano/microfibers, which possess dual properties separately derived from the core and

the sheath materials, via a simple, versatile single-step coaxial electrospinning process. Teflon AF, as a kind of amorphous fluoropolymer, is widely used to fabricate hydrophobic surfaces. However, such hydrophobic fluoropolymers are not spinnable in general due to their low dielectric constant. In virtue of poly(ε-caprolactone) (PCL) as core materials, the Teflon fibers were firstly obtained via a simple one-step coaxial electrospinning. The combination of the spinnable core polymer enhancing surface roughness with none spinnable Teflon AF fluoropolymer lowering low surface energy has contributed to superhydrophobicity. Such coaxial electrospinning has gained more and more attraction in the field of composite materials, allowing many potential applications, such as protective clothing, filtration membranes and so on (**Figure17**).

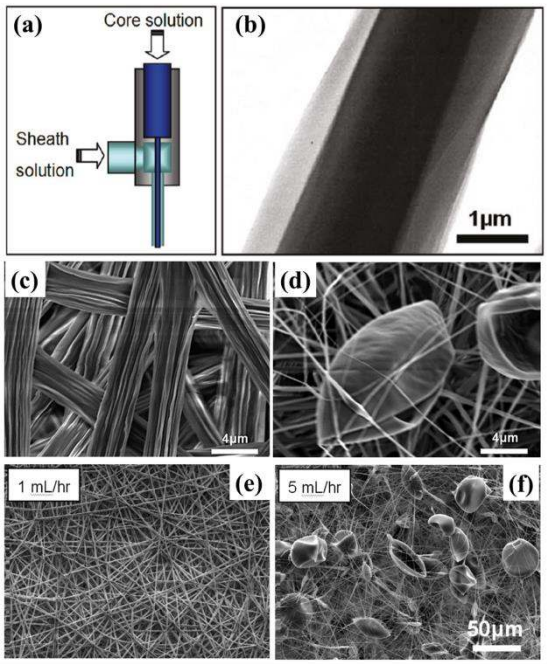

Figure 17. Coaxial electrospinning operation: (a) diagram of the coaxial nozzle; (b) PCL/Teflon fiber TEM cross-section; Morphology of PCL/Teflon fibers obtained with different PCL concentrations: (c) PCL 10 wt.% with 1.5 mL/h and Teflon 1 wt.% with 1.0 mL/h; (d) PCL 7 wt.% with 1.4 mL/h and Teflon 1 wt.% with 1.4 mL/h. Electric

field for all samples: 500 V/cm; Effect of Teflon sheath solution flow rate on fiber morphologies, (e) 1 mL/h, (f) 5 mL/h. Reproduced with permission from [107]. Copyright 2009 American Chemical Society.

5. Functional applications

On account of the outstanding properties of superamphiphobic surfaces and the increasing demand for such materials, more and more attention has been paid on their multifunctional applications with great progress made.[17, 52] The following will focus on the new functions that the superamphiphobic surfaces have brought about.

5.1. Droplets manipulation

The generation and manipulation of micro/nano-liter droplets has gained immense interest in various fields, such as biosensing, inkjet printing, microfluidics, microreactor engineering and so on. Huang et al. have realized droplet manipulation on patterned superamphiphobic TiO_2 films by introducing ink layers to increase localized adhesion between solid and liquid. Four typical micro-droplet manipulations, viz. storage, moving, mixing and transfer, are displayed in Figure 18. In Figure 18c, 10 μL droplets in array could be stably stored in 1.0 mm ink dots even though they were placed vertically and upside down. Droplets transportation could easily be achieved on such patterned surfaces on account of the adhesion contrast (**Figure 18**d,e). Figure 20f has displayed a “V” shape formed by the meeting of MO droplets (methyl orange) and acid water droplets in same end point, which were mounted along two different lines. In addition to the droplets mixing action on one surface,

droplets could also realize contact, react and assay on two substrates (**Figure 18**g). Moreover, on basis of the high adhesion contrast, drops could be transferred to another targeted surface with no loss (**Figure 18**h). A line pattern could be designed ahead of time on the substrates, allowing droplets to slide along the path through a slight vibration or simple titling (**Figure 18**i).[136] Jiang et al.[137] utilized the superamphiphobic surfaces with controllable oil adhesion to develop an oil droplet-based microreactor to manipulate oil droplets. By adjusting external preload forces or surface morphology, the surface adhesion of oil could be modulated, allowing oil droplets to transport in a drop-to-drop system. During this experiment, the first oil droplet with styrene monomers was picked up from a low adhesive superamphiphobic surface to put in a metal cap. Subsequently, this droplet began to react with another one that contained Br_2 on a high adhesion surface. Finally, these two droplets merged into one droplet and reacted with each other resulting in high adhesion. Such superamphiphobic surfaces with adjustable oil adhesion promise many potential applications in droplet transportation, microfluidic systems and so on. In their subsequent work,[138] they have designed a superamphiphobic nozzle for the successful manipulation of some organic droplets. On account of the super-repellency to liquids on the surface of this nozzle, oil droplet was avoided spreading and restricted at the edge of the nozzle, resulting in a high transfer efficiency for liquids. Moreover, 3D structures could be constructed by dispensing oil-based inks with the superamphiphobic nozzle directly, which is greatly significant for the development of ink-jet printing and liquid transportation fields. Very recently, Wong et al.[139] have

designed a superamphiphobic bionic proboscis (SAP) for manipulating simple or complicated core-shell nano-liter droplets inspired by the fluid manipulation of butterflies. Such superamphiphobic proboscises were prepared via a rapid gas-nanotexturing process on both the internal and external surfaces of hypodermic needles. The SAPs enable the generation and release of ultra-small droplets with very low surface tensions (**Figure 18**j-o). The rapid fabrication of self-contained micro-reactors was so unprecedented an achievement that it allowed immediate applications in biology and chemistry fields.

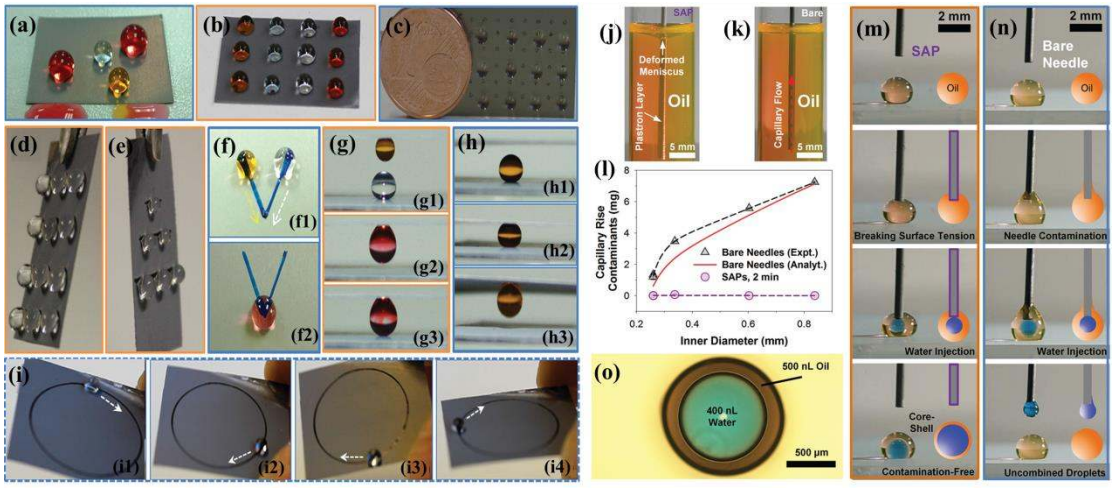

Figure18. (a) The unstable liquid droplets on uniform superamphiphobic AHT surface. (b) The stable liquid droplet arrays on visible ink covering patterns. The implementation of the adhesion contrast on the dynamic manipulation of some typical micro-droplet based on the ink patterned superamphiphobic AHT surfaces: (c) storage, (d,e) moving, (f,g) mixing, (h,i) transfer.[136] Contamination-free manipulation of core-shell droplets. Immersion of (j) a SAP and (k) a bare needle in tetradecane oil showcasing the contamination-free properties of the SAPs. (l) Analysis of contamination of SAPs (circles) and bare needles (triangles) and their theoretical

estimate (line) by capillary rise as a function of the gauge size from 18 to 26 G. (m) Demonstration of the facile in-air synthesis of core–shell oil-water nanoliter droplets with the SAPs. Droplet injection using a SAP showcasing the superamphiphobic needle's superior contamination-free insertion of a nanoliter water droplet within an oil drop shell. In contrast, (n) bare needles are not able to synthesize core–shell droplets due to adhesion of the water droplet to the needle surface. (o) Microscope image of an in-air core-shell 400 nL water droplet in a 500 nL oil droplet demonstrating unique control of complex droplet structures. Reproduced with permission from [139]. Copyright 2017 Wiley.

5.2. Anti-fouling

Considering many practical applications, such as clothing, kitchenware, oil pipeline and so on, anti-fouling property is of great significance in a wide range of areas.[140-143] Yuan et al.[144] have prepared the superamphiphobic coating with composite ethylene tetrafluoroethylene-polyaniline functionalized carbon nanotubes. Such a liquid-repellent surface was able to keep the surface uncontaminated even after immersion test for 100 cycles in the sludge, while the blank aluminum plate was seriously covered with dirt after the first immersion. In the sludge drop test, simulated sludge, made of a hybrid of ethyl glycerol / water (1:9, v/v) mixture and extremely corrosive high concentration H_2SO_4 (98%) solution, could rapidly slip down from the coating, leaving behind a clean surface. Even after many cycles of the test, the water contact angles maintained about 160° (**Figure 19**a1-e). In the meanwhile, Chen et al.[99] have synthesized a kind of flower-shaped superamphiphobic FOTS-TiO_2

powder (1H,1H,2H,2H-perfluorooctyltrichloro silane) with outstanding anti-fouling property. As for oil-fouling resistance, the treated glass was dipped into the peanut oil, slightly agitated, and then taken out of the oily environment. Between the liquid and solid phase, an entrapped air layer was clearly observed, resulting in a neat surface without any oil residue. Besides the hard substrate, soft porous material was also treated with FOTS-TiO_2 coating, showing excellent anti-fouling performance as well. As exhibited in **Figure 19**f,g, the blank and treated cottons were immersed into the water dyed with methyl blue. A marked contrast could be observed, in which the blank cottons were completely soaked and turned blue color, while the coated cottons could still keep white without any contamination. The obtained anti-fouling ability is so outstanding that it promises this coating various industrial applications even under harsh environment.

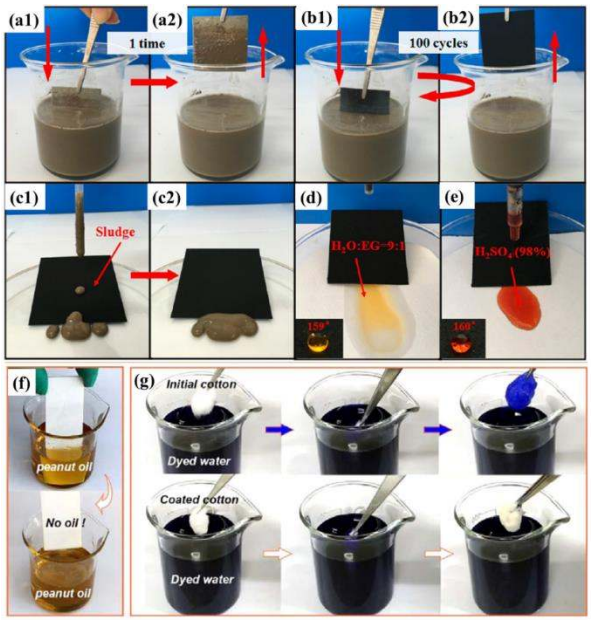

Figure 19. Antifouling tests of uncoated aluminum plate (a1, a2) and ETFE-PANI/fCNTs-6 composite coating (b1, b2) by immersion into sludge. Non-wetting tests with sludge (c1, c2), mixture of H_2O and ethylene glycol (EG) (d),

and concentrated H_2SO_4 (e). Reproduced with permission from [144]. Copyright 2016 American Chemical Society. (f) Coated glass slide was dipped into the peanut oil and brought out without any oil. (g) Non-treated cotton was completely dyed into blue in the methyl-blue-dyed water. Treated cotton was not dyed and still remains white after immersing. Reproduced with permission from [99]. Copyright 2016 American Chemical Society.

5.3. Oil/water separation

Nowadays, many urgent problems such as the drilling and purification of oil, as well as the treatment and recycling of wastewater have caused severe environmental problems and threatened human health. Hence, a simple oil-water separation process with high efficiency and low energy consumption, especially those driven by gravitational force only, is needed.[145-149] Ge et al.[120] have reported a liquid pre-wetting technique to develop a multifunctional gravity-driven separator, which is capable of selective removal of water or oil from oil–water mixtures or emulsions (**Figure 20**a-d). A two-step pre-wetting procedure was always required to achieve the selective separation. Firstly, the superamphiphobic paper sample was pre-wetted with ethanol, which has a lower surface energy than water and the oil used, to drive out air in the porous cellulose network. Next, water or oil was introduced to replace ethanol depending on which liquid would be removed later. Such a facile, versatile separator with high separation flux and high separation efficiency promises a bright future in various practical applications. Lin et al. have developed a superamphiphobic coating by a facile dip-coating method using a hybrid of SiO_2 and heptadecafluorononanoic

acid-modified TiO_2 sol.[150] Such a coating can turn superhydrophilic and superoleophobic upon exposure to ammonia, thereby realizing oil/water separation. Common materials, such as polyurethane sponge and polyester fabric, can be used as substrates, displaying unique capabilities of controlling the filtration of an oil–water mixture and selectively removing water from oil (**Figure 20**e,f). Such novel coating can greatly advance the oil-water separation techniques, promising various practical applications and many effective solutions of emergent environmental concerns.

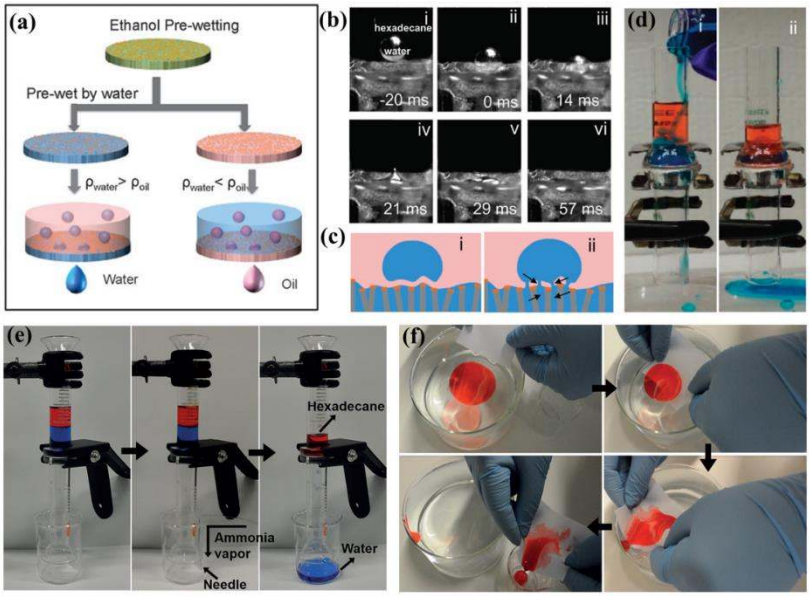

Figure 20. (a) Schematic illustration of selective separation of oil-water mixtures. (b) Time lapse photos of a water droplet transferred on water prewetted SA-paper in the hexadecane phase. (c) Illustrations of (i) formation and (ii) breaking of the disjoining layer, corresponding to water transportation shown in (a-iii). Red, blue, orange and grey colors stand for hexadecane, water, stringed NP layer and cellulose fiber. (d) Separation of free hexadecane–water mixtures. During (i) and after (ii) separation, hexadecane is dyed red and water is dyed blue for better visualization. Reproduced with permission from [120]. Copyright 2015 The Royal Society of Chemistry. (e)

Oil-water separation by the functionalized polyester fabric. (f) Snapshots showing the collection of hexadecane floating on the water surface using an ammonia-exposed, superhydrophilic, and superoleophobic polyester fabric. Reproduced with permission from [150]. Copyright 2015 Wiley.

5.4. Patterning

In most cases, uniform surfaces with unique wettability or adhesion contrast are always suitable for precise and reliable patterning design.[77, 151-153] Inspired by the precise regulation of chemical component and surface morphology of natural organisms, Lai et al.[154] have constructed patterned superamphiphobic anatase TiO_2 particles (ATP) films, which can be erased and rewritten easily, for biomedical applications and microfluidic management. By combining UV illumination with self-assembly process, the wettability pattern can be quickly removed and regenerated on the ATP surface. In contrast to a mass of reports on uniform super-repellent surfaces with uncontrollable sliding behavior (**Figure 21**d) or super-repellent surfaces with large wetted areas (**Figure 21**e), they also demonstrated the patterned super-repellent surfaces with minimal contact area and controllable adhesion through the introduction of high energy chemical component to specific pots (**Figure 21**f). And they applied a facile electrochemical anodizing technique to produce wetting patterns by covering a site-selective ink on the TiO_2 nanotube array surface.[152] Very recently, they have created wetting micropatterns by using a photomask to achieve wettability transition process on the fabrics surfaces (**Figure 21**j). The micropatterning process has been displayed in **Figure 21**i.[153] Lin et al. have

fabricated a patterned electrically conductive superamphiphobic coating on textiles surfaces via a facile one-step vapour-phase polymerization process.[130] In this experiment, patterns could be easily generated on polypyrrole-fluorinated alkyl silane coatings surface via a screen-printing method to terminate the polymerization process in the particular region. The obtained patterns could be applied to form a circuit to drive electronic devices (**Figure 21**a-c). Different from the previously reported construction for patterns based on the asymmetric wettability, Dong et al.[120] have used various cationic dyes, such as ABR, methylene blue and basic yellow, to prepared the comparably superamphiphobic coatings with different colors. Just as the "rocket" in **Figure 21**g,h, colorful superamphiphobic patterns can be obtained by simple spray process in virtue of a mask. Such multicolored patterned superamphiphobic coatings with robust durability may be of great value in various fields, such as the restoration of cultural relics and anti-creeping of oils.

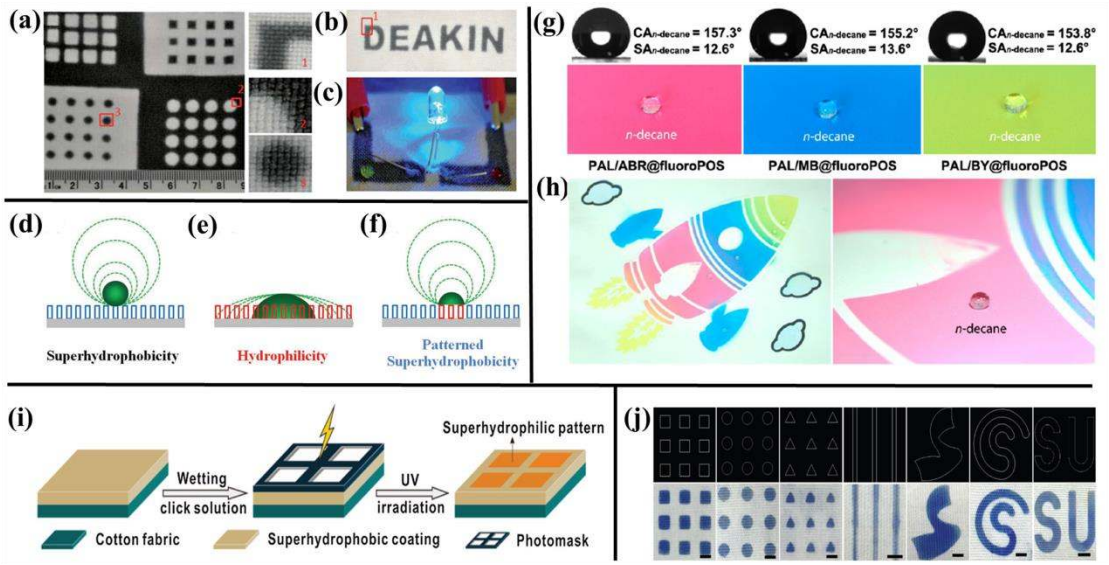

Figure 21. (a) Examples of PPy–FAS patterns, (b) a letter PPy–FAS pattern, (c) a simple PPy–FAS circuit for lighting a LED device, with coloured water (green) and

hexadecane (red) droplets on the working PPy–FAS surface. Reproduced with permission from [130]. Copyright 2011 The Royal Society of Chemistry. Schematics of side-view profiles for various drop volumes on a (d) homogenous superhydrophobic (CA≥150°) surface, (e) hydrophilic (CA≤90°) surface, and (f) surface with patterned superhydrophobic pattern. Reproduced with permission from [152]. Copyright 2013 Wiley. Images of (g) the superamphiphobic coatings prepared using different cationic dyes with n-decane droplets on them and (h) a multicolored superamphiphobic "rocket" pattern. C_{PAL} = 15 g L^{-1}; $C_{PFDTES\text{-}i}$ = 22.7 mM; C_{TEOS} = 8.9 mM; $C_{PFDTES\text{-}ii}$ = 7.6 mM. Reproduced with permission from [120]. Copyright 2016 American Chemical Society. (i) Schematic presentation of fabrication of micropatterns, layout, and optical images infiltrated by dyed deionized water; (j) squares, circles, triangles, stripes, and other self-defined logo patterns. Scale bars are 2 mm. Reproduced with permission from [153]. Copyright 2017 Wiley.

5.5. Fluid carrier device

Water striders can walk on water freely and quickly, during which their feet float above water to minimize the resistance while stay dry.[155] As shown in **Figure 22**a-c, Jiang and his co-workers have revealed that the legs of water striders are super-repellant owing to a layer of hydrophobic wax material with hierarchical micro/nano-structures on them.[156, 157] Inspired by water striders, Jin et al. have developed superamphiphobic nanocellulose aerogel membranes composed of fibrillar networks, which could be used as cargo carriers on water and oil.[158] The obtained membranes have displayed good permeability, high adhesion and almost unchanged

viscous drag (**Figure 22**d-h). Furthermore, such cargos were capable of supporting a weight almost 1000 times of its own weight. Lai et al.[154] have prepared superamphiphobic Ti substrates, which were coated with anatase TiO_2 particles (ATP) and subsequently functionalized with 1H,1H,2H,2H-perfluorodecyltriethoxysilane (PFDS). Such surfaces displayed superoleophobic in air but underwater superoleophilic, and could act as "oil capture hands" to collect oil droplets (**Figure 22**i,j). The obtained plates could absorb oil droplets in water. Once they moved out of water, the oil droplets can be easily separated from the surface due to the superoleophobicity in air. Such material can be applied to the collection of oils in water with a high efficiency. They also prepared dual-scale hierarchical TiO_2 films to transport oil droplets between superoleophobic surfaces under water, followed by spreading on targeted underwater superoleophilic surface on basis of conversed wettability and adhesion with environment-responsive property (**Figure 22**k1-k4).[159]

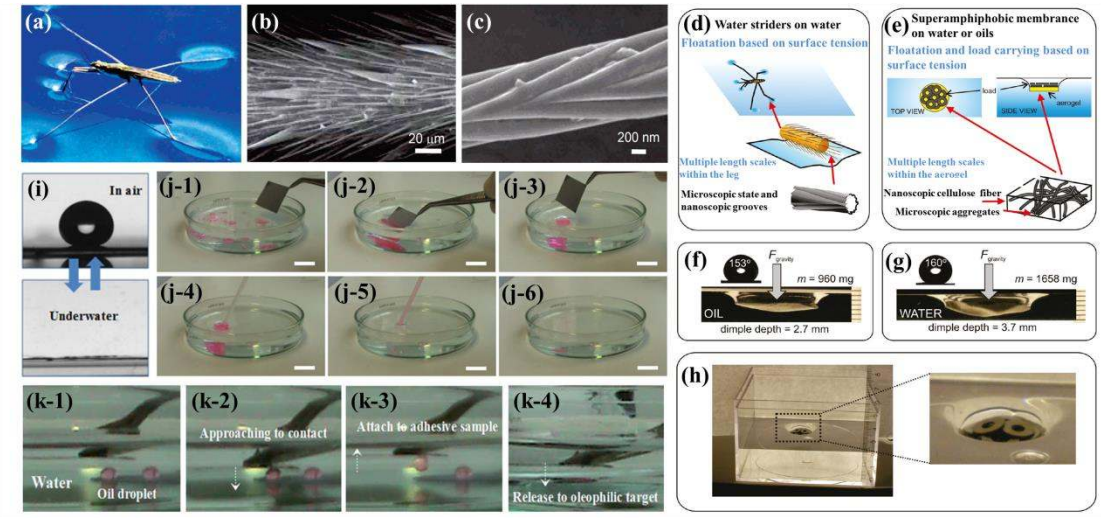

Figure 22. (a) Water strider resting on water. (b) SEM images of a water strider leg covered by numerous oriented needle-shaped microsetae. (c) SEM image of grooved nanostructure on the seta surface. Reproduced with permission from [157]. Copyright

2007 American Chemical Society. Floatation and load carrying on oil and water based on fluorinated nanostructured aerogel. (d) Inspiration came from water striders, a class of insects capable of floating on water based on surface tension, using superhydrophobic legs with fibrillar structures. (e) Cartoon of a fluorinated nanofibrous cellulose aerogel membrane floating on water and oil due to surface tension. As in water striders, also in the aerogels the topography for liquid repellency is induced by fibers, but in this case the fibers form mechanically robust entangled networks. (f,g) Contact angle measurement and load carrying experiment of the aerogel on, respectively, paraffin oil and water. The side-view photograph of the aerogel load carrier on paraffin oil and water shows the dimple at maximum supportable weight. The scale markers on the right are in millimeters. (h) Load carrying setup. Metal weights (washers) are loaded on the fluorinated aerogel membrane floating on water (similarly on oil). Reproduced with permission from [158]. Copyright 2011 American Chemical Society. (i) The oil droplet image on the PFDS modified ATP surface in air or underwater environment. (j) The oil capture and collection process with a superoleophobic plate and underwater superoleophilic property. Process 1–2: a superoleophobic plate touches and captures the underwater oil drops sprayed in bottom of a glass container. Process 3: the captured oil drops gathered together underwater as the superoleophobic plate moves out. Process 4–6: the gathered oil droplets are collected from the water. The oil was colored pink for convenient observation through the capture and collection process. Reproduced with permission from [154]. Copyright 2013 Nature. (k1–k4) Typical underwater oil droplet

dyed pink with the 1,2-dichloroethane transportation process by taking advantage of the extreme high adhesion contrast of the underwater superoleophobic surface. Reproduced with permission from [159]. Copyright 2014 American Chemical Society.

5.6. Self-cleaning

Lotus leaf is known to possess outstanding self-cleaning ability. Water fluids can slide away and carry the dirt away from the leaf surface, thereby making it clean (**Figure 23**b).[160, 161] Inspired by lotus leaf, researchers have successfully developed a variety of materials with self-cleaning property, many of which have been put into practice, like exterior walls and windshields. On account of the high CA and low SA for water and oil, superamphiphobic surfaces can show extraordinary self-cleaning capacity for both water and oil fluids. Zhao et al. have fabricated a superamphiphobic silicon wafer surface with directional self-cleaning ability via the combination of photolithography and subsequent modification.[162] The anisotropic self-cleaning property could be obtained due to the parallel grooves structures on the surface. Extremely similar to butterfly wings, the droplets can move rapidly in the parallel direction but are blocked in the vertical direction. Furthermore, the aforementioned flower-like superamphiphobic FOTS-TiO_2 powder synthesized by Chen et al. has also displayed self-cleaning property.[99] Qing et al. have demonstrated an ultra-robust superamphiphobic surface with self-cleaning property via a facile metal electrodeposition and subsequent coating with fluorinated metal-oxide nanoparticles. Astonishingly, such surface could retain the outstanding self-cleaning property even after oil contamination and 50 abrasion cycles with sandpaper (**Figure 23**a-f).[163] Qu

et al.[164] have fabricated three different super-repellent surfaces, the superhydrophobic, superamphiphobic, and superoleophobic-superhydrophilic materials by modifying kaolin particles. They have evaluated the self-cleaning performance of the three types of coatings by placing them separately in a slightly inclined watch glass with methyl blue powders as the model dust. As shown in **Figure 23**c, the powder on the superhydrophobic material surface was immediately picked up, dissolved and carried away by water, leaving behind a clear surface. The initial transparent water gradually becomes turbid. The water droplets still retained a spherical shape when they were rolling away with the dirt, which explained the key role of the low water sliding angle and low surface energy in a self-cleaning process. In contrast to the previous material, the oil droplet could roll down the superoleophobic-superhydrophilic surface and pick up the dusts with no effect on its motion (**Figure 23**d). Similarly, both water and oil droplets were able to get rid of dusts on the superamphiphobic materials (**Figure 23**e).

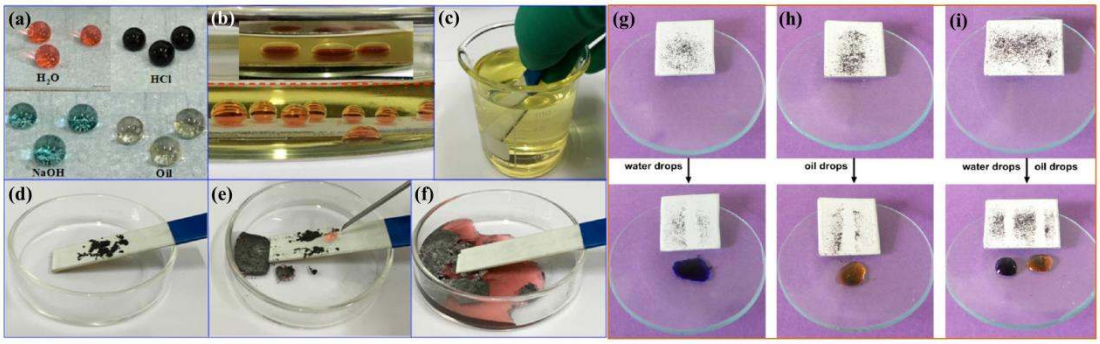

Figure 23. Self-cleaning effect of the FAS-TiO_2/Zn surface (superamphiphobic surface) after 50th abrasion cycle with sandpaper. (a) Different types of liquid droplets with spherical shape on superamphiphobic surface: red-colored H_2O droplet, black-colored HCl droplet, blue-colored NaOH droplet, and oil droplet. (b)

Red-colored H_2O droplets sitting on the FAS-TiO_2/Zn surface under oil (lower image) and on rough electrodeposited Zn surface (upper image). (c−f) Self-cleaning process of the superamphiphobic surface after being contaminated by oil. Reproduced with permission from [163]. Copyright 2017 American Chemical Society. Self-cleaning performance of (g) superhydrophobic, (h) superoleophobic-superhydrophilic, and (i) superamphiphobic materials are tested with methyl blue powder. Reproduced with permission from [164]. Copyright 2016 American Chemical Society.

5.7. Anti-icing

For a long time, anti-icing property is still a technological challenge for some high-tech devices or outdoor infrastructures like radar, space flight and aviation vehicles. From a scientific perspective, the anti-icing property can be evaluated from several aspects: the constrained expansion of ice film, the delay in the crystallization of condensed water and the removal of water/condensed water before it freezes.[165-167] Wang et al.[168] have prepared anti-icing superhydrophobic surfaces, followed by the water dropping test and the artificial steam-freezing test. When a droplet was dropped onto the blank steel surface under overcooled conditions, it just stayed, spread and then froze on the surface because of the hydrophilic nature. However, the droplet could roll off easily on the super-repellent surface quickly before freezing occurs. In a steam-freezing test, a large ice film was formed on the blank steel, while no ice film or even very small freezing spots could be observed on the coated surface (**Figure 24**a-f). Such a freezing delay could be ascribed to the lower water freezing point on the super-repellent surface owing to micro/nano scale hierarchical structures. In the

work by Chen et al.,[99] it has been proved that the prepared superamphiphobic FOTS-TiO_2 coating can display good ice delay and icephobic performances on the sponge substrate. Freezing of a water droplet took about 19 min on the blank half of the sponge, while it took nearly 1 h for the droplet to freeze on the treated half. The combination of low thermal conductivity of sponge with small solid−liquid contact area has contributed to such outstanding ice-delay performance. In addition, the ice droplets could easily drop down from the treated half surface by simple extrusion process, whereas the ice droplets just adhered to the untreated half (**Figure 24**g).

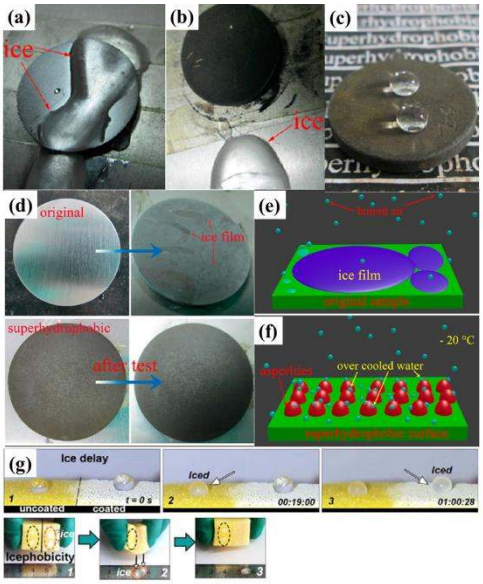

Figure 24. Comparison of the icing film on (a) original steel and (b) A6 surface. (c) Water droplets on A6 after the dripping test under overcooled condition. The surface still exhibited lotus-like water repellency. (d) Comparison of frost films on A6 after the steam-freezing (from 50°C with 90% humidity to the −20°C condition) test. Schematic view of the condensed small droplets on (e) original steel and (f) A6 surface. Reproduced with permission from [168]. Copyright 2015 American Chemical Society. (g) The powder-coated sponge is capable of delaying ice formation and

reducing ice adhesion. Reproduced with permission from [99]. Copyright 2016 American Chemical Society.

5.8. Corrosion resistance

In a humid environment, metals and their alloys easily get oxidized and corroded, which has caused many serious problems such as accelerated aging of the products, environmental pollution and enormous waste, thereby greatly limiting their applications.[8] Superamphiphobic surfaces may be an effective solution to such problems because the super-antiwetting coating can effectively isolate the metals from the corrosive media. Jiang's group[132, 169] employed an electrochemical reaction to endow some engineering metals and their alloys like Zn, Al, Fe, Ni and Zn–Fe alloy with superamphiphobicity, promising strong anti-corrosion property for practical use. Yuan et al. have fabricated superamphiphobic coatings on common cast iron surfaces.[170] There were no rust, weight and color changes on the prepared metal substrates even after half a year in the ambient atmosphere, whereas great changes could be observed on the original metal surface. In addition, Zhang et al.,[171] have also prepared superamphiphobic Al surface via the combination of simple HCl etching with subsequent PFOA functionalization. In another work from the same group,[172] corrosion-resistant superamphiphobic coatings on copper sheets surface were constructed through Ag deposition and surface fluorination. The damaged superamphiphobic surfaces could be easily recovered through a simple regeneration process. There is hope of practical production in a large scale for this coated surfaces. Motlagh et al. have fabricated robust superamphiphobic films on stainless steel

substrates with corrosion resistance.[173] The obtained surface could preserve its superamphiphobic property even after 16-day immersion in water with the protection efficiency of 97.33%.

5.9. Other special superamphiphobic surfaces

5.9.1. Transparent surface

Optical transparent materials that are repellent to various liquids including water and oils are very useful in our daily life, such as touch screens, eye-glasses, building windows and windshields, where transparency and super-repellency are both vital for their functions. As surface roughness is indispensable for the construction of superamphiphobicity, however a rough surface is going to affect the required transparency.[174] This is because the transmittance will decrease with the increase of roughness on account of light scattering.[8, 175] Hence, optimizing the surface roughness is the key to obtain transparent superamphiphobic surfaces. In recent years, diverse templates have been employed to prepare robust transparent superamphiphobic coatings.[160, 176]

Deng et al.[160] have designed a transparent superamphiphobic surface by virtue of candle soot as a template. The ultraviolet-visible transmittance spectra was employed to verify the transparency (**Figure 25**a1,3). In contrast to the blank glass surface, the transmittance of the obtained superamphiphobic surface decreased by lower than 10% at the wavelengths of 500 nm. Ganesh et al.[176] have utilized another template, viz. SiO_2 nanofibers, to prepare transparent superamphiphobic coating by electrospining. The obtained surfaces displayed CAs of 161° and 146.5° towards

water and hexadecane droplets, respectively. The transmittance of the coated glass was measured to be 85% by ultraviolet-visible transmittance spectra. Such transmittance makes it applicable to many applications like building windows (**Figure 25a**2,4). A translucent superamphiphobic coating has been prepared on paper by Li et al.[177] with more than 45% of transmittance in the visible range, thereby resulting in the almost unchanged visibility of the characters on the paper under the glass. Moreover, the liquids with various surface tensions, ranging from water to some organic liquids, have exhibited nearly spherical shapes on the coated surface. Hence, such facile technique may provide the translucent superamphiphobic paper with large-scale commercial applications.

5.9.2. Surfaces with controllable wettability and adhesion

Plasma surface treatment can be used to achieve the wettability transition. Ellinas et al. have fabricated an ordered, triple-scale, PMMA polymer substrates via microparticle colloidal lithography.[178] The surface displayed amphiphilicity after treated with O_2 plasma, while it became amphiphobic through fluorocarbon plasma treat. Photoresponsive switch is another facile way to control wettability. Zhang et al.[179] have described superamphiphobic perfluorosilane-rendered TiO_2/single-walled carbon nanotube composite coatings (**Figure 25**b). UV irradiation was applied to gradually decompose fluorosilane on the composite coating surface, thereby realizing the wettability switch from superoleophobic to superhydrophilic. It is interesting to observe that liquids with surface tension gap within 5 mN/m can achieve complete opposite wetting states on one surface through the control of the UV irradiation dose,

which means superphobicity for one droplet but superphilicity for another with lower surface tension. The mixtures of various liquids with different surface tension could realize separation through a treated mesh. Kim et al.[180] have also employed UV irradiation to achieve the conversion from high oil-repellency to amphiphilicity.

Controlling droplets adhesion has also played a fundamental role in many practical applications of surfaces with special wettability. It is difficult to realize the transition between low and high adhesion due to the irreversible switch from Wenzel's to Cassie's state. Lai et al.[181] have made a summary of recent advances in TiO_2-based nanostructured surfaces with controllable wettability and adhesion and proposed current challenges and future prospects of this renascent and rapidly developing field. Yao et al.[137] have reported a facile technique to construct superamphiphobic coatings via perfluorothiolate reaction on $Cu(OH)_2$ nanostructure surfaces. The obtained surfaces displayed controllable oil adhesive force on basis of surface nanostructures or external preloads on the oil droplet.

5.9.3. Asymmetric surface

Asymmetric surfaces can show directional wetting behavior for liquids. Droplets can be repelled from one super-antiwetting side, while they just can be absorbed on the other side. Achieving the asymmetric wetting properties is of great significance for function engineering to fabricate self-cleaning, comfortable, breathable, and less skin-irritating surfaces. Wang et al.[182] have reported a novel superamphiphobic surface by a two-step coating process using flowerlike ZnO nanorods, fluorinated decyl polyhedral oligomeric silsesquioxanes, and hydrolyzed fluorinated alkylsilane.

Once one side was exposed to UV irradiation, the obtained fabric displayed asymmetric property and achieved a one-way transport for oil fluid automatically from the unexposed side to the irradiated side, while it just spread on the surface in an opposite direction without fluid transport (**Figure 25**c). Liu et al.[77] have employed an electrospraying method to realize asymmetric wetting with one side displaying highly anti-wetting behavior and the other side retaining the inherent hydrophilic and oleophilic nature of the pristine cotton fabric. Based on this special wettability, the obtained fabric could display a one-way directional transport feature.

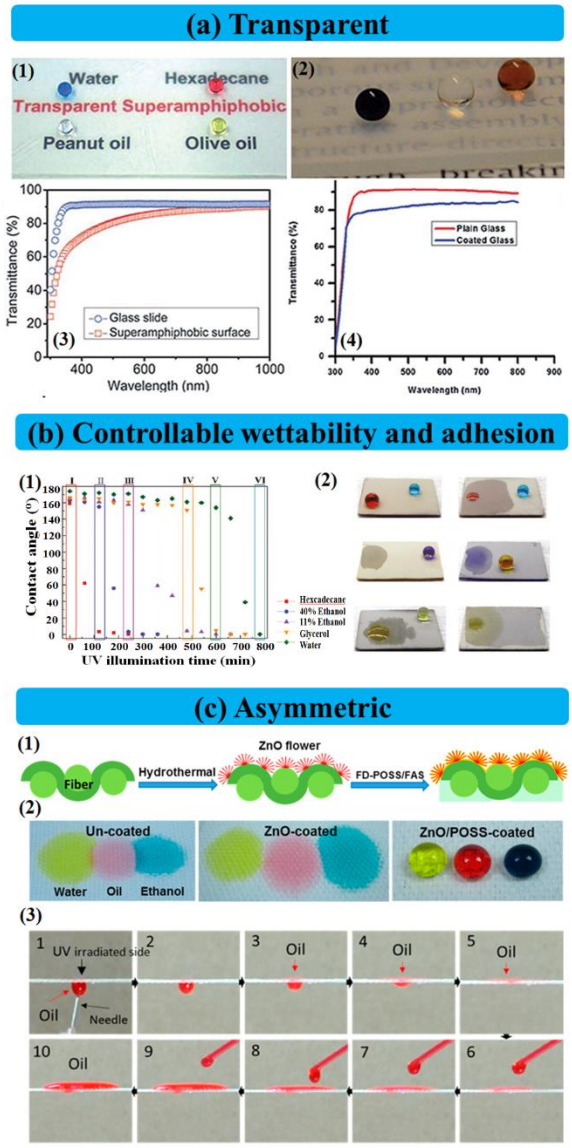

Figure 25. (a) Transparent surface: Image of (1) a drop of dyed water, dyed hexadecane, peanut oil and olive oil deposited on a superamphiphobic glass slide, Reproduced with permission from [160]. Copyright 2012 Science. (2) blue-dyed water, red-dyed hexadecane and colorless ethylene glycol droplets on the superamphiphobic surface. Reproduced with permission from [176]. Copyright 2013 The Royal Society of Chemistry. Ultraviolet-visible transmittance spectra of (3) 3 mm thick superamphiphobic surface compared with pristine glass, Reproduced with permission from [160]. Copyright 2012 Science. (4) superamphiphobic coated glass surface compared with a plain surface. Reproduced with permission from [176]. Copyright 2013 The Royal Society of Chemistry. (b) Surfaces with controllable wettability and adhesion: Wettability tuning of the TiO_2/SWNT (single-walled carbon nanotube) coating using UV irradiation. (1) Contact angles (θ*) for various liquids, including hexadecane, 40% ethanol, 11% ethanol, glycerol, and water as a function of UV irradiation time. Windows I-VI correspond to the surface states in which a liquid pair can be distinguished by complete converse wetting behavior on the coating surface. (2) Wetting behavior of liquid pairs on the coating with surface wetting states corresponding to windows I-VI in (1). Reproduced with permission from [179]. Copyright 2011 American Chemical Society. (c) Asymmetric surface: (1) coating procedure, (2) photographs of yellow-colored water, red-colored cooking oil, and blue-colored ethanol (volume 35 μL) on cotton fabrics. (3) Still frames taken from a video to show the dropping of red-dyed cooking oil onto the UV-irradiated "front" and "back" surfaces. Reproduced with permission from [182]. Copyright 2015

American Chemical Society.

6. Conclusions and outlooks

In this article, we mainly focus an overview of the recent progress on superamphiphobic surfaces by summarizing the typical creatures, basic characterization, common fabrications and functional applications. The development of these surfaces is vital for fundamental research, as well as for various commercial applications. Through persistent endeavor for many years, tremendous achievements have been made in this area. However, a variety of challenges still exist and demand prompt solutions before industrial production and practical use are realized. For example, most of the fabrication techniques are only limited to laboratory study rather than mass production. In order to fulfill the crucial demand of practical applications, enhancing mechanical stability of superamphiphobic coatings may be another problem in need of urgent solution. However, only sparse study work was reported about this aspect. So we need to grasp this good opportunity to prepare robust superamphiphobic surfaces. Furthermore, self-healing property of superamphiphobic surface may be a future trend in this area because of its potential promise in practical use. Once their superhydrophobicity or superoleophobicity is damaged after long-time use, these properties should be easily restored. Many a time, raw materials with high cost or environmental hazard have hindered the practical application of the developed superamphiphobic products. Hence, it is essential to build suitable super-antiwetting surfaces with lower-cost and environmental-friendliness in mind.

In order to overcome the aforementioned problems, we should take the following aspects into consideration. Firstly, it is extremely valuable to carry out fundamental research on superamphiphobic surfaces, particularly on morphology design. Next, the technique with simple operation and easy repeatability is very vital. Then, the superamphiphobic surfaces with mechanical resistance to various harsh environments should be given priority. Last but not least, non-toxic, inexpensive and common materials should be selected for mass production. Generally speaking, a broad space for the development of superamphiphobic surfaces exists. And we believe a promising future in this field will emerge for the design and construction of such surfaces because of their huge potential in increasing productivity and saving cost in various aspects of human activities.

Conflicts of interest

There are no conflicts to declare.

Acknowledgements

The authors thank the National Natural Science Foundation of China (21501127 and 51502185), Nantong Science and Technology Project (GY12016030), Jiangsu Advanced Textile Engineering Center Project (Project No. SPPGO[2014]22), and the funds from the Priority Academic Program Development of Jiangsu Higher Education Institutions (PAPD).

References

[1] S. T. Wang, K. S. Liu, X. Yao, L. Jiang, *Chem. Rev.* **2015,** *115*, 8230.

[2] K. S. Liu, M. Y. Cao, A. Fujishima, L. Jiang, *Chem. Rev.* **2014,** *114*, 10044.

[3] K. S. Liu, X. Yao, L. Jiang, *Chem. Soc. Rev.* **2010,** *39*, 3240.

[4] T. Young, *Philos. Trans. R. Soc.* **1805,** *95*, 65.

[5] M. J. Liu, Y. M. Zheng, J. Zhai, L. Jiang, *Acc. Chem. Res.* **2010,** *43*, 368.

[6] K. S. Liu, L. Jiang, *Nano Today* **2011,** *6*, 155.

[7] J. X. Wang, Y. Z. Zhang, S. T. Wang, Y. L. Song, L. Jiang, *Acc. Chem. Res.* **2011,** *44*, 405.

[8] X. Yao, Y. L. Song, L. Jiang, *Adv. Mater.* **2011,** *23*, 719.

[9] T. L. Sun, G. Y. Qing, B. L. Su, L. Jiang, *Chem. Soc. Rev.* **2011,** *40*, 2909.

[10] F. Xia, L. Jiang, *Adv. Mater.* **2008,** *20*, 2842.

[11] Z. Zhu, S. Zheng, S. Peng, Y. Zhao, Y. Tian, *Adv. Mater.* **2017,** *29*, 1703120.

[12] G. Ding, W. Jiao, R. Wang, Y. Niu, L. Hao, F. Yang, W. Liu, *J. Mater. Chem. A*. **2017,** *5*, 17325.

[13] H. Ollivier, *J. Phys. Theor. Appl.* **1907,** *6*, 757.

[14] F. Bartell, J. Shepard, *J. Phys. Chem.* **1953,** *57*, 455.

[15] W. Barthlott, C. Neinhuis, *Planta* **1997,** *202*, 1.

[16] X. Zhang, F. Shi, J. Niu, Y. G. Jiang, Z. Q. Wang, *J. Mater. Chem.* **2008,** *18*, 621.

[17] A. Tuteja, W. Choi, M. L. Ma, J. M. Mabry, S. A. Mazzella, G. C. Rutledge, G. H. McKinley, R. E. Cohen, *Science* **2007,** *318*, 1618.

[18] H. J. Li, X. B. Wang, Y. L. Song, Y. Q. Liu, Q. S. Li, L. Jiang, D. B. Zhu, *Angew.*

Chem.-Int. Edit. **2001,** *40*, 1743.

[19] G. R. Artus, J. Zimmermann, F. A. Reifler, S. A. Brewer, S. Seeger, *Appl. Surf. Sci.* **2012,** *258*, 3835.

[20] J. Y. Huang, Y. K. Lai, F. Pan, L. Yang, H. Wang, K. Q. Zhang, H. Fuchs, L. F. Chi, *Small* **2014,** *10*, 4865.

[21] L.-P. Xu, J. Peng, Y. Liu, Y. Wen, X. Zhang, L. Jiang, S. Wang, *ACS Nano* **2013,** *7*, 5077.

[22] J. Yang, H. Song, B. Chen, H. Tang, C. Li, *RSC Adv.* **2014,** *4*, 14227.

[23] S. H. Li, T. X. Zhu, J. Y. Huang, Q. Q. Guo, G. Q. Chen, Y. K. Lai, *Int. J. Nanomed.* **2017,** *12*, 2593.

[24] A. Siriviriyanun, T. Imae, *Chem. Eng. J.* **2014,** *246*, 254.

[25] H. Zhao, K.-Y. Law, *Langmuir* **2012,** *28*, 11812.

[26] B. Su, Y. Tian, L. Jiang, *J. Am. Chem. Soc.* **2016,** *138*, 1727.

[27] H. Liu, S. Gao, J. Cai, C. He, J. Mao, T. Zhu, Z. Chen, J. Huang, K. Meng, K. Zhang, Y. Lai, *Materials* **2016,** *9*, 124.

[28] M. Qu, S. Liu, J. He, J. Feng, Y. Yao, L. Hou, X. Ma, X. Liu, *RSC Adv.* **2016,** *6*, 79238.

[29] S. Zhang, J. Huang, Z. Chen, Y. Lai, *Small* **2017,** *13*, 1602992.

[30] M. Im, H. Im, J.-H. Lee, J.-B. Yoon, Y.-K. Choi, *Soft Matter* **2010,** *6*, 1401.

[31] H. Zhao, K.-C. Park, K.-Y. Law, *Langmuir* **2012,** *28*, 14925.

[32] T. J. Li, M. Paliy, X. L. Wang, B. Kobe, W. M. Lau, J. Yang, *ACS Appl. Mater. Inter.* **2015,** *7*, 10988.

[33] S. Nishimoto, B. Bhushan, *RSC Adv.* **2013,** *3*, 671.

[34] B. Bhushan, in *Biomimetics*, Springer **2016,** *pp*. 23.

[35] T. Darmanin, F. Guittard, *Mater. Today* **2015,** *18*, 273.

[36] A. K. Epstein, B. Pokroy, A. Seminara, J. Aizenberg, *Proceedings of the National Academy of Sciences* **2011,** *108*, 995.

[37] R. Rakitov, S. N. Gorb, *Proc. Natl Acad. Sci.* **2013,** *280*, 20122391.

[38] R. Helbig, J. Nickerl, C. Neinhuis, C. Werner, *PloS one* **2011,** *6*, e25105.

[39] R. Hensel, R. Helbig, S. Aland, H.-G. Braun, A. Voigt, C. Neinhuis, C. Werner, *Langmuir* **2013,** *29*, 1100.

[40] J. Nickerl, R. Helbig, H.-J. Schulz, C. Werner, C. Neinhuis, *Zoomorphology* **2013,** *132*, 183.

[41] J. Nickerl, M. Tsurkan, R. Hensel, C. Neinhuis, C. Werner, *J. R. Soc. Interface* **2014,** *11*, 20140619.

[42] K. Liu, Y. Tian, L. Jiang, *Prog. Mater. Sci.* **2013,** *58*, 503.

[43] P. S. Brown, B. Bhushan, *Sci. Rep.* **2016,** *6*, 21048.

[44] R. Hensel, C. Neinhuis, C. Werner, *Chem. Soc. Rev.* **2016,** *45*, 323.

[45] J. Genzer, K. Efimenko, *Biofouling* **2006,** *22*, 339.

[46] R. N. Wenzel, *Ind. Eng. Chem. Res.* **1936,** *28*, 988.

[47] A. Cassie, S. Baxter, *Trans. Farad. Soc.* **1944,** *40*, 546.

[48] L. Feng, Y. Zhang, J. Xi, Y. Zhu, N. Wang, F. Xia, L. Jiang, *Langmuir* **2008,** *24*, 4114.

[49] M. Jin, X. Feng, L. Feng, T. Sun, J. Zhai, T. Li, L. Jiang, *Adv. Mater.* **2005,** *17*,

1977.

[50] A. Tuteja, W. Choi, M. Ma, J. M. Mabry, S. A. Mazzella, G. C. Rutledge, G. H. McKinley, R. E. Cohen, *Science* **2007,** *318*, 1618.

[51] A. Tuteja, W. Choi, J. M. Mabry, G. H. McKinley, R. E. Cohen, *Proc. Natl Acad. Sci.* **2008,** *105*, 18200.

[52] J. Zhang, S. Seeger, *Angew. Chem.-Int. Edit.* **2011,** *50*, 6652.

[53] S. Pan, A. K. Kota, J. M. Mabry, A. Tuteja, *J. Am. Chem. Soc*. **2012,** *135*, 578.

[54] T. Y. Liu, C. J. Kim, *Science* **2014,** *346*, 1096.

[55] T. S. Wong, S. H. Kang, S. K. Y. Tang, E. J. Smythe, B. D. Hatton, A. Grinthal, J. Aizenberg, *Nature* **2011,** *477*, 443.

[56] Z. L. Chu, S. Seeger, *Chem. Soc. Rev.* **2014,** *43*, 2784.

[57] K.-H. Cho, L.-J. Chen, *Nanotechnology* **2011,** *22*, 445706.

[58] G. R. Artus, S. Jung, J. Zimmermann, H. P. Gautschi, K. Marquardt, S. Seeger, *Adv. Mater.* **2006,** *18*, 2758.

[59] T.-S. Wong, S. H. Kang, S. K. Tang, E. J. Smythe, B. D. Hatton, A. Grinthal, J. Aizenberg, *Nature* **2011,** *477*, 443.

[60] Y. Huang, J. Zhou, B. Su, L. Shi, J. Wang, S. Chen, L. Wang, J. Zi, Y. Song, L. Jiang, *J. Am. Chem. Soc.* **2012,** *134*, 17053.

[61] M. Kuang, J. Wang, B. Bao, F. Li, L. Wang, L. Jiang, Y. Song, *Adv. Opt. Mater.* **2014,** *2*, 34.

[62] J. Zimmermann, S. Seeger, F. A. Reifler, *Text. Res. J.* **2009,** *79*, 1565.

[63] P. S. Brown, B. Bhushan, *Sci. Rep.* **2016,** *6*, 21048.

[64] L. Cao, T. P. Price, M. Weiss, D. Gao, *Langmuir* **2008,** *24*, 1640.

[65] W. Choi, A. Tuteja, S. Chhatre, J. M. Mabry, R. E. Cohen, G. H. McKinley, *Adv. Mater.* **2009,** *21*, 2190.

[66] A. Tuteja, W. Choi, G. H. McKinley, R. E. Cohen, M. F. Rubner, *MRS bulletin* **2008,** *33*, 752.

[67] L. Joly, T. Biben, *Soft Matter* **2009,** *5*, 2549.

[66] R. T. Rajendra Kumar, K. B. Mogensen, P. Bøggild, *J. Phys. Chem. C.* **2010,** *114*, 2936.

[69] Y. Liu, Y. Xiu, D. W. Hess, C. Wong, *Langmuir* **2010,** *26*, 8908.

[70] S. Srinivasan, S. S. Chhatre, J. M. Mabry, R. E. Cohen, G. H. McKinley, *Polymer* **2011,** *52*, 3209.

[71] T. Wu, Y. Suzuki, *Sens. Actuators. B.* **2011,** *156*, 401.

[72] J. Yang, Z. Zhang, X. Men, X. Xu, X. Zhu, *New. J. Chem.* **2011,** *35*, 576.

[73] H. Zhao, K.-Y. Law, V. Sambhy, *Langmuir* **2011,** *27*, 5927.

[74] Z. Geng, J. H. He, L. Yao, *RSC Adv.* **2015,** *5*, 89262.

[75] Z. Geng, J. H. He, *J. Mater. Chem. A* **2014,** *2*, 16601.

[76] X. Du, Y. Xing, X. Y. Li, H. W. Huang, Z. Geng, J. H. He, Y. Q. Wen, X. J. Zhang, *RSC Adv.* **2016,** *6*, 7864.

[77] H. Liu, J. Y. Huang, F. Y. Li, Z. Chen, K. Q. Zhang, S. S. Al-Deyab, Y. K. Lai, *Cellulose* **2017,** *24*, 1129.

[78] C. Y. Cao, M. Z. Ge, J. Y. Huang, S. H. Li, S. Deng, S. N. Zhang, Z. Chen, K. Q. Zhang, S. S. Al-Deyab, Y. K. Lai, *J. Mater. Chem. A*, **2016,** *4*, 12179.

[79] H. D. Wang, H. Zhou, A. Gestos, J. Fang, T. Lin, *ACS Appl. Mater. Interfaces*, **2013,** *5*, 10221.

[780] H. Zhou, H. X. Wang, H. T. Niu, A. Gestos, T. Lin, *Adv. Funct. Mater.* **2013,** *23*, 1664.

[81] C. Schlaich, L. C. Carnacho, L. X. Yu, K. Achazi, Q. Wei, R. Haag, *ACS Appl. Mater. Inter.* **2016,** *8*, 29117.

[82] S.-I. Chang, J.-B. Yoon, *Opt. Express* **2004,** *12*, 6366.

[83] J.-H. Lee, W.-S. Choi, K.-H. Lee, J.-B. Yoon, *J. Micromech. Microeng.* **2008,** *18*, 125015.

[84] J.-H. Lee, H.-S. Lee, B.-K. Lee, W.-S. Choi, H.-Y. Choi, J.-B. Yoon, *Optics letters* **2007,** *32*, 2665.

[85] X. J. Huang, J. H. Lee, J. W. Lee, J. B. Yoon, Y. K. Choi, *Small* **2008,** *4*, 211.

[86] X. J. Huang, D. H. Kim, M. Im, J. H. Lee, J. B. Yoon, Y. K. Choi, *Small* **2009,** *5*, 90.

[87] H. Zhao, K.-Y. Law, *ACS Appl. Mater. Inter.* **2012,** *4*, 4288.

[88] T. Darmanin, F. Guittard, S. Amigoni, E. T. de Givenchy, X. Noblin, R. Kofman, F. Celestini, *Soft Matter* **2011,** *7*, 1053.

[89] K. Ellinas, S. P. Pujari, D. A. Dragatogiannis, C. A. Charitidis, A. Tserepi, H. Zuilhof, E. Gogolides, *ACS Appl. Mater. Inter.* **2014,** *6*, 6510.

[90] L. Li, V. Breedveld, D. W. Hess, *ACS Appl. Mater. Inter.* **2013,** *5*, 5381.

[91] S. Peng, X. J. Yang, D. Tian, W. L. Deng, *ACS Appl. Mater. Inter.* **2014,** *6*, 15188.

[92] X. W. Li, T. Shi, C. Liu, Q. X. Zhang, X. J. Huang, *Sci. Rep.* **2016,** *6*, 35940.

[93] N. Wang, D. S. Xiong, Y. L. Deng, Y. Shi, K. Wang, *ACS Appl. Mater. Inter.* **2015,** *7*, 6260.

[94] S. Barthwal, Y. S. Kim, S. H. Lim, *Langmuir* **2013,** *29*, 11966.

[95] J. Xu, K. Jang, J. Lee, H. J. Kim, J. Jeong, J. G. Park, S. U. Son, *Cryst. Growth Des.* **2011,** *11*, 2707.

[96] H. Wang, Z. G. Guo, *Appl. Phys. Lett.* **2014,** *104*, 4.

[97] J. W. Zeng, Z. G. Guo, *Colloid Surf. A* **2014,** *444*, 283.

[98] Q. F. Yao, C. Wang, B. T. Fan, H. W. Wang, Q. F. Sun, C. D. Jin, H. Zhang, *Sci. Rep.* **2016,** *6*, 35505.

[99] L. W. Chen, Z. G. Guo, W. M. Liu, *ACS Appl. Mater. Inter.* **2016,** *8*, 27188.

[100] J. Yu, H. J. Wang, N. Q. Yin, X. L. Xu, *RSC Adv.* **2014,** *4*, 24163.

[101] L. K. Gao, S. L. Xiao, W. T. Gan, X. X. Zhan, J. Li, *RSC Adv.*, **2015,** *5*, 98203.

[102] Z. Guo, W. Liu, B.-L. Su, *J. Colloid. Interf. Sci.* **2011,** *353*, 335.

[103] J. D. Ferguson, E. R. Smith, A. W. Weimer, S. M. George, *J. Electrochem. Soc.* **2004,** *151*, G528.

[104] S. Rezaei, I. Manoucheri, R. Moradian, B. Pourabbas, *Chem. Eng. J.* **2014,** *252*, 11.

[105] M. Paven, R. Fuchs, T. Yakabe, D. Vollmer, M. Kappl, A. N. Itakura, H. J. Butt, *Adv. Funct. Mater.* **2016,** *26*, 4914.

[106] F. Li, M. Du, Q. Zheng, *Acs Nano* **2016,** *10*, 2910.

[107] D. W. Han, A. J. Steckl, *Langmuir* **2009,** *25*, 9454.

[108] A. S. Nair, S. Yang, P. Zhu, S. Ramakrishna, *Chem. Commun.* **2010,** *46*, 7421.

[109] Y. Shengyuan, Z. Peining, A. S. Nair, S. Ramakrishna, *J. Mater. Chem.* **2011,** *21*, 6541.

[110] P. N. Zhu, A. S. Nair, S. J. Peng, S. Y. Yang, S. Ramakrishna, *ACS Appl. Mater. Inter.* **2012,** *4*, 581.

[111] Z. Peining, A. S. Nair, Y. Shengyuan, P. Shengjie, N. K. Elumalai, S. Ramakrishna, *J. Photochem. Photobiol. A Chem.* **2012,** *231*, 9.

[112] A. K. Kota, Y. X. Li, J. M. Mabry, A. Tuteja, *Adv. Mater.* **2012,** *24*, 5838.

[113] F. E. Ahmed, B. S. Lalia, N. Hilal, R. Hashaikeh, *Desalination* **2014,** *344*, 48.

[114] V. A. Ganesh, S. S. Dinachali, A. S. Nair, S. Ramakrishna, *ACS Appl. Mater. Inter.* **2013,** *5*, 1527.

[115] S. J. Pan, A. K. Kota, J. M. Mabry, A. Tuteja, *J. Am. Chem. Soc.* **2013,** *135*, 578.

[116] H. X. Wang, Y. H. Xue, J. Ding, L. F. Feng, X. G. Wang, T. Lin, *Angew. Chem.-Int. Edit.* **2011,** *50*, 11433.

[117] E. S. Medeiros, G. M. Glenn, A. P. Klamczynski, W. J. Orts, L. H. C. Mattoso, *J. Appl. Polym. Sci.* **2009,** *113*, 2322.

[118] B. C. Li, J. P. Zhang, *Chem. Commun.* **2016,** *52*, 2744.

[116] D. T. Ge, L. L. Yang, C. B. Wang, E. Lee, Y. Q. Zhang, S. Yang, *Chem. Commun.* **2015,** *51*, 6149.

[119] J. Dong, Q. Wang, Y. J. Zhang, Z. Q. Zhu, X. H. Xu, J. P. Zhang, A. Q. Wang, *ACS Appl. Mater. Inter.* **2017,** *9*, 1941.

[121] J. P. Zhang, B. Yu, Z. Q. Gao, B. C. Li, X. Zhao, *Langmuir* **2017,** *33*, 510.

[122] S. Srinivasan, S. S. Chhatre, J. M. Mabry, R. E. Cohen, G. H. McKinley,

Polymer **2011,** *52*, 3209.

[123] D. Xiong, G. J. Liu, L. Z. Hong, E. J. S. Duncan, *Chem. Mater.* **2011,** *23*, 4357.

[124] G. W. Zhang, S. D. Lin, I. Wyman, H. L. Zou, J. W. Hu, G. J. Liu, J. D. Wang, F. Li, F. Liu, M. L. Hu, *ACS Appl. Mater. Inter.* **2013,** *5*, 13466.

[125] T. Darmanin, F. Guittard, *J. Colloid Interface Sci.* **2009,** *335*, 146.

[126] T. Darmanin, F. Guittard, *Chem. Commun.* **2009,** 2210.

[127] T. Darmanin, F. Guittard, *J. Am. Chem. Soc.* **2009,** *131*, 7928.

[128] H. Bellanger, T. Darmanin, F. Guittard, *Langmuir* **2012,** *28*, 186.

[129] J. Y. Huang, S. H. Li, M. Z. Ge, L. N. Wang, T. L. Xing, G. Q. Chen, X. F. Liu, S. S. Al-Deyab, K. Q. Zhang, T. Chen, Y. K. Lai, *J. Mater. Chem. A* **2015,** *3*, 2825.

[130] H. X. Wang, Y. H. Xue, T. Lin, *Soft Matter* **2011,** *7*, 8158.

[131] H. X. Wang, H. Zhou, A. Gestos, J. Fang, H. T. Niu, J. Ding, T. Lin, *Soft Matter* **2013,** *9*, 277.

[132] J. M. Xi, L. Feng, L. Jiang, *Appl. Phys. Lett.* **2008,** *92*, 053102.

[133] H. F. Meng, S. T. Wang, J. M. Xi, Z. Y. Tang, L. Jiang, *J. Phys. Chem. C* **2008,** *112*, 11454.

[134] C. Pereira, C. Alves, A. Monteiro, C. Magen, A. M. Pereira, A. Ibarra, M. R. Ibarra, P. B. Tavares, J. P. Araujo, G. Blanco, J. M. Pintado, A. P. Carvalho, J. Pires, M. F. R. Pereira, C. Freire, *ACS Appl. Mater. Inter.* **2011,** *3*, 2289.

[135] D. Kim, H. Im, M. J. Kwak, E. Byun, S. G. Im, Y. K. Choi, *Sci. Rep.* **2016,** *6*, 25456.

[136] J. Y. Huang, Y. K. Lai, F. Pan, L. Yang, H. Wang, K. Q. Zhang, H. Fuchs, L. F.

Chi, *Small* **2014,** *10*, 4865.

[137] X. Yao, J. Gao, Y. L. Song, L. Jiang, *Adv. Funct. Mater.* **2011,** *21*, 4270.

[138] L. Wu, Z. C. Dong, N. Li, F. Y. Li, L. Jiang, Y. L. Song, *Small* **2015,** *11*, 4837.

[139] W. S. Y. Wong, G. Liu, A. Tricoli, *Small* **2017,** *13*, 1603688.

[140] G. Y. Wang, H. R. Wang, Z. G. Guo, *Chem. Commun.* **2013,** *49*, 7310.

[141] K. Sivashanmugan, P. C. Liu, K. W. Tsai, Y. N. Chou, C. H. Lin, Y. Chang, T. C. Wen, *Nanoscale* **2017,** *9*, 2865.

[142] B. Bhushan, P. Muthiah, *Microsyst. Technol.* **2013,** *19*, 1261.

[143] P. Muthiah, B. Bhushan, K. Yun, H. Kondo, *J. Colloid Interface Sci.* **2013,** *409*, 227.

[144] R. X. Yuan, S. Q. Wu, P. Yu, B. H. Wang, L. W. Mu, X. G. Zhang, Y. X. Zhu, B. Wang, H. Y. Wang, J. H. Zhu, *ACS Appl. Mater. Inter.* **2016,** *8*, 12481.

[145] Z. Wang, Y. Wang, G. Liu, *Angew. Chem.-Int. Edit.* **2016,** *55*, 1291.

[146] Q. Zhu, Q. Pan, F. Liu, *J. Phy. Chem.* **2011,** *115*, 17464.

[147] L. Feng, Z. Y. Zhang, Z. H. Mai, Y. M. Ma, B. Q. Liu, L. Jiang, D. B. Zhu, *Angew. Chem.-Int. Edit.* **2004,** *43*, 2012.

[148] J. Yuan, X. Liu, O. Akbulut, J. Hu, S. L. Suib, J. Kong, F. Stellacci, *Nature Nanotech.* **2008,** *3*, 332.

[149] Z. Xue, S. Wang, L. Lin, L. Chen, M. Liu, L. Feng, L. Jiang, *Adv. Mater.* **2011,** *23*, 4270.

[150] Z. G. Xu, Y. Zhao, H. X. Wang, X. G. Wang, T. Lin, *Angew. Chem.-Int. Edit.* **2015,** *54*, 4527.

[151] Y. K. Lai, L. X. Lin, F. Pan, J. Y. Huang, R. Song, Y. X. Huang, C. J. Lin, H. Fuchs, L. F. Chi, *Small* **2013,** *9*, 2945.

[152] Y. Lai, F. Pan, C. Xu, H. Fuchs, L. Chi, *Adv Mater* **2013,** *25*, 1682.

[153] S. Deng, J. Huang, Z. Chen, Y. Lai, *Adv. Mater. Inter.* **2017,** *4*, 1700268.

[154] Y. K. Lai, Y. X. Tang, J. Y. Huang, F. Pan, Z. Chen, K. Q. Zhang, H. Fuchs, L. F. Chi, *Sci. Rep.* **2013,** *3*, 3009.

[155] M. A. Samaha, H. V. Tafreshi, M. Gad-el-Hak, *C. R. Mec.* **2012,** *340*, 18.

[156] T. L. Sun, L. Feng, X. F. Gao, L. Jiang, *Acc. Chem. Res.* **2005,** *38*, 644.

[157] X. Q. Feng, X. F. Gao, Z. N. Wu, L. Jiang, Q. S. Zheng, *Langmuir* **2007,** *23*, 4892.

[158] H. Jin, M. Kettunen, A. Laiho, H. Pynnonen, J. Paltakari, A. Marmur, O. Ikkala, R. H. A. Ras, *Langmuir* **2011,** *27*, 1930.

[159] J. Huang, Y. Lai, L. Wang, S. Li, M. Ge, K. Zhang, H. Fuchs, L. Chi, *J. Mater. Chem. A* **2014,** *2*, 18531.

[160] X. Deng, L. Mammen, H. J. Butt, D. Vollmer, *Science* **2012,** *335*, 67.

[161] Y. D. Wang, N. Lu, H. B. Xu, G. Shi, M. J. Xu, X. W. Lin, H. B. Li, W. T. Wang, D. P. Qi, Y. Q. Lu, L. F. Chi, *Nano. Res.* **2010,** *3*, 520-.

[162] H. Zhao, K. Y. Law, *Langmuir* **2012,** *28*, 11821.

[163] Y. Qing, C. Hu, C. Yang, K. An, F. Tang, J. Tan, C. Liu, *ACS Appl. Mater. Inter.* **2017,** *9*, 16571.

[164] M. Qu, X. Ma, J. He, J. Feng, S. Liu, Y. Yao, L. Hou, X. Liu, *ACS Appl. Mater. Inter.* **2017,** *9*, 1011.

[165] P. Tourkine, M. Le Merrer, D. Quere, *Langmuir* **2009,** *25*, 7214.

[166] M. He, Q. L. Zhang, X. P. Zeng, D. P. Cui, J. Chen, H. L. Li, J. J. Wang, Y. L. Song, *Adv. Mater.* **2013,** *25*, 2291.

[167] S. A. Kulinich, M. Farzaneh, *Appl. Surf. Sci.* **2009,** *255*, 8153.

[168] N. Wang, D. Xiong, Y. Deng, Y. Shi, K. Wang, *ACS Appl. Mater. Inter.* **2015,** *7*, 6260.

[169] T. Darmanin, F. Guittard, *Langmuir* **2009,** *25*, 5463.

[170] Z. Q. Yuan, J. Y. Xiao, C. Q. Wang, J. C. Zeng, S. L. Xing, J. Liu, *J. Coat. Technol. Res.* **2011,** *8*, 773.

[171] J. Yang, Z. Z. Zhang, X. H. Xu, X. H. Men, X. T. Zhu, X. Y. Zhou, *New J. Chem.* **2011,** *35*, 2422.

[172] Z. Z. Zhang, X. T. Zhu, J. Yang, X. H. Xu, X. H. Men, X. Y. Zhou, *Appl. Phys.* **2012,** *108*, 601.

[173] N. V. Motlagh, F. C. Birjandi, J. Sargolzaei, N. Shahtahmassebi, *Appl. Surf. Sci.* **2013,** *283*, 636.

[174] P. Mazumder, Y. D. Jiang, D. Baker, A. Carrilero, D. Tulli, D. Infante, A. T. Hunt, V. Pruneri, *Nano Lett.* **2014,** *14*, 4677.

[175] H. M. Shang, Y. Wang, S. J. Limmer, T. P. Chou, K. Takahashi, G. Z. Cao, *Thin Solid Films* **2005,** *472*, 37.

[176] V. A. Ganesh, S. S. Dinachali, H. K. Raut, T. M. Walsh, A. S. Nair, S. Ramakrishna, *RSC Adv.* **2013,** *3*, 3819.

[177] J. Li, L. Yan, Q. L. Ouyang, F. Zha, Z. J. Jing, X. Li, Z. Q. Lei, *Chem. Eng. J.*

2014, *246*, 238.

[178] K. Ellinas, A. Tserepi, E. Gogolides, *Langmuir* **2011,** *27*, 3960.

[179] M. Zhang, T. Zhang, T. H. Cui, *Langmuir* **2011,** *27*, 9295.

[180] T. I. Kim, D. Tahk, H. H. Lee, *Langmuir* **2009,** *25*, 6576.

[181] Y. Lai, J. Huang, Z. Cui, M. Ge, K. Q. Zhang, Z. Chen, L. Chi, *Small* **2016,** *12*, 2203.

[182] H. X. Wang, H. Zhou, W. D. Yang, Y. Zhao, J. Fang, T. Lin, *ACS Appl. Mater. Inter.* **2015,** *7*, 22874.

Yandong Wang received his PhD degree in the field of physical chemistry from Jilin University in 2013. After that, he joined Prof. Chi's group in Muenster University first and then Soochow University as a postdoctoral fellow. His current research interests focus on fabrication of nanostructures and their application in optical and photonic fields based on colloidal lithography.

Jianying Huang received her Ph.D. degree in 2007 from the Department of Materials, Xiamen University. During 2007–2011, she worked as an assistant professor at Fujian Institute of Research on the Structure of Matter. After that, she moved to Muenster University as a visiting scholar. She is currently an associate professor at National Engineering Laboratory for Modern Silk, and School of Textile and Clothing Engineering in Soochow University since 2013. Her research interests focus on the bio-inspired intelligent surfaces with superwettability, ATRP and click-chemistry reactions.

Yuekun Lai is a professor in the College of Textile and Clothing Engineering at Soochow University, with joint appointments in the National Engineering Laboratory for Modern Silk from 2013. He obtained Ph.D. degree from the Department of Chemistry, Xiamen University. During 2009–2011, he worked as a research fellow at the School of Materials Science and Engineering, Nanyang Technological University, Singapore. In 2011, he moved to Muenster University under the support of the Humboldt Foundation Scholarship of Germany. His current research topics are bio-inspired intelligent materials with special wettability, multifunctional fabrics, and TiO_2 nanostructures for energy & environmental applications.

Bioinspired from the nature, a detailed account of the innovative fabrication and further fundamental research of superamphiphobicity are summarized with highlight on the recent progress and comparison. Subsequently, the new functions that the superamphiphobic surfaces have brought about have been reviewed, which involve in droplets manipulation, anti-fouling, patterning, fluid carrier device and so on.

Keyword： superwettability, superamphiphobicity, re-entrant geometries, innovative fabrication, fundamental research

Hui Liu, Yandong Wang*, Jianying Huang*, Zhong Chen, Guoqiang Chen, and Yuekun Lai*

Bioinspired surfaces with superamphiphobic properties: Concepts, synthesis and applications